European Journal of Medicinal Chemistry 163 (2019) 671–689

Contents lists available at ScienceDirect

European Journal of Medicinal Chemistry

journal homepage: http://www.elsevier.com/locate/ejmech

Research paper

Discovery and optimization of a series of 3-substituted indazole derivatives as multi-target kinase inhibitors for the treatment of lung squamous cell carcinoma

Qi Wang [a, c, 1], Yang Dai [b, 1], Yinchun Ji [b, 1], Huanyu Shi [a, c], Zuhao Guo [a, c], Danqi Chen [a], Yuelei Chen [a], Xia Peng [b], Yinglei Gao [b], Xin Wang [a], Lin Chen [a], Yuchen Jiang [b, c], Meiyu Geng [b, c], Jingkang Shen [a], Jing Ai [b, c, **], Bing Xiong [a, c, *]

[a] Department of Medicinal Chemistry, Shanghai Institute of Materia Medica, Chinese Academy of Sciences, 555 Zuchongzhi Road, Shanghai, 201203, China
[b] Division of Anti-tumor Pharmacology, State Key Laboratory of Drug Research, Shanghai Institute of Materia Medica, Chinese Academy of Sciences, 555 Zuchongzhi Road, Shanghai, 201203, China
[c] University of Chinese Academy of Sciences, NO.19A Yuquan Road, Beijing, 100049, China

ARTICLE INFO

Article history:
Received 25 September 2018
Received in revised form
4 December 2018
Accepted 6 December 2018
Available online 7 December 2018

Keywords:
Squamous cell carcinoma
Multi-target inhibitor
DDR
FGFR

ABSTRACT

Although lung adenocarcinoma patients have benefited from the development of targeted therapy, patients with lung squamous cell carcinoma (SqCC) have no effective treatment due to the complexity and heterogeneity of the disease. Therefore, basing on the genetic analysis of mutations in lung squamous cell carcinoma to design multi-target inhibitors represents a potential strategy for the medical treatment. In this study, through screening an in-house focused library, we identified an interesting indazole scaffold. And following with binding analysis, we elaborated the structure-activity relationship of this hit compound by optimizing four parts guided by the DDR2 enzymatic assay, which resulted in a potent lead compound **10a**. We conducted further optimization of dual enzymatic inhibitions towards FGFR1 and DDR2, two important kinases in lung squamous cell carcinoma. Finally, from the cellular antiproliferative activity tests and in vivo pharmacokinetic test, 3-substituted indazole derivative **11k** was found to be a promising candidate and subjected to in vivo pharmacology study with the mouse xenograft models, demonstrating profound anti-tumor efficacy. Additional in vitro druglike assessment reinforced that compound **11k** could be valuable for SqCC drug development.

1. Introduction

Lung cancer is the leading cause of cancer-related death worldwide, accounting for about one-quarter of all cancer deaths and in USA alone resulting more than 150,000 people deaths annually. Despite of the great advances in lung cancer treatment, the five-year survival rate of lung cancer has not been improved significantly over the last three decades, and remains only about 5%, which poses a grand challenge for drug development [1]. The predominant subtype of lung cancer is non-small cell lung cancer (NSCLC), covering approximately 80%–85% of all lung cancers [2]. Adenocarcinoma (ADC, approximately 40–50% of cases) and squamous cell carcinoma (SqCC, approximately 20–30%) are the main histological subtypes of NSCLC [3]. Along with the advances of human genomics and post-genomics technologies, comprehensive target identifications have been launched for better understanding the pathology of non-small cell lung cancer. Various oncogenic-driven proteins in NSCLC were validated as drug targets, and many small-molecule drugs targeting these onco-proteins have been approved by FDA, such as gefitinib, afatinib and osimertinib for EGFR mutants (15%), ceritinib and alectinib for ALK rearrangement (5%), vemurafenib, dafrafenib and trametinib for BRAF-V600E mutants (1–3%) [4]. However, these targeted drugs have largely been confined to patients with adenocarcinoma of NSCLC. While in the case of SqCC, the drug development is lagged behind due to the

* Corresponding author. Department of Medicinal Chemistry, Shanghai Institute of Materia Medica, Chinese Academy of Sciences, 555 Zuchongzhi Road, Shanghai, 201203, China.
** Corresponding author. Division of Anti-tumor Pharmacology, State Key Laboratory of Drug Research, Shanghai Institute of Materia Medica, Chinese Academy of Sciences, 555 Zuchongzhi Road, Shanghai, 201203, China.
E-mail addresses: jai@simm.ac.cn (J. Ai), bxiong@simm.ac.cn (B. Xiong).
[1] These authors contributed equally.

https://doi.org/10.1016/j.ejmech.2018.12.015
0223-5234/

poor understanding the pathology of this specific subtype of NSCLC, and the standard first-line therapy is still limited to the platinum-based chemotherapy [5].

SqCC is an intricate and heterogeneous disease and most genetic alternations found in cell cycle regulation and squamous differentiation are belong to receptor tyrosine kinases (RTK) related signaling pathways [6]. Statistically, about 50–80% of SqCC have a known oncogenic driver mutation [7], these mutations in receptors or protein kinases can stimulate a complex cascade of signaling pathways such as the RAS-RAF-MEK-ERK or MAPK, PI3K-AKT-mTOR or JAK-STAT pathways. In the last decade, genetic aberrances identified and characterized in SqCC mainly include PIK3CA mutation, FGFR1 amplification, PDGFR-α amplification/mutation and DDR2 mutation [8]. However, the relationship between the single genetic alteration and therapeutic response is not always straightforward and other factors also play important roles in modulating the response to a targeted therapy [9]. For example, FGFR1 amplified tumors were dependent on FGF ligands and increased ligand levels led to reduced sensitivity to FGFR1 inhibition; dasatinib treated lung squamous cells could bypassed activating a panel of RTKs and their signaling adaptor complexes [10]; Generally, these frequent occurring mutations in driver genes implicated the complexity of personalized therapy in SqCC [11,12]. Therefore, rational drug discovery for more effective multi-target inhibitors may be necessary to treat SqCC patients. And among them, we are particularly interested in two RTKs, Fibroblast Growth Factor Receptor 1 (FGFR1) and Discoindin Domain Receptor 2 (DDR2), due to their important roles in SqCC.

FGFR1 is one of the most frequently amplified genes in human cancer. Activation of FGFR1 led by endogenous ligand binding initializes three downstream pathways: the Ras-MAP kinase pathway, the PI3K-Akt-mTOR pathway and PLCγ-Ca^{2+} pathway to control cell proliferation, survival and differentiation [13]. Additionally, FGFR1 amplification occurs frequently in SqCC and can serve as a negative prognostic marker in patients with early-stage SqCC [14].s.

The discoindin domain receptor (DDR2) is a non-integrin-type receptor in collagen-mediated signaling with tyrosine kinase activity [15]. DDR2 plays a critical role as regulator for epithelial–mesenchymal transition [16] and participates in cross-talk with other cell surface receptors such as integrins and insulin-like growth factor-1 receptor [17]. When interacts with the collagen in the extracellular matrix, the DDR2 was activated, further adhered the cell-cell connections, remodeled the extracellular matrix, transduced the signals in the cell and finally increased the cell proliferation [18]. Recent studies indicated that continuous activation of DDR2, whether through mutation or overexpression, was frequently found in SqCC lung cancer cell lines. And inhibition of DDR2 activity can suppress collagen-induced colony formation and cell proliferation. Utilizing the sequencing method, Hammerman et al. found that DDR2 mutations, similar to the incidence of EML-ALK in lung adenocarcinomas, are present in 4% of lung SqCCs [12] and most of these mutants are oncogenic and associated with gain-of-function phenotype of cancer transformation, providing solid evidence to select DDR2 as the drug target for SqCC lung cancer.

In the present study, we initially placed our efforts on optimizing the DDR2 activity, because of its importance in SqCC and limited reports of DDR2 inhibitors. To identify new chemotypes, we screened an in-house focused kinase library against DDR2 in an enzymatic assay. After obtaining the hit compound and probing the interaction mode with first round of structural modification, we regarded it binding to DDR2 as type II kinase inhibitor. Then, systematic SAR study was conducted to optimize the DDR2 inhibition activity. After obtaining the lead compound **10a**, we intended to optimize the DDR2 and FGFR1 activities simultaneously and revealed that N-substituted pyrazole played an important role in improving the potency to FGFR1 and DDR2, as well as the cellular antiproliferation activity. Finally, on the basis of the bioactivities and in vivo pharmacokinetic profiles, compound **11k** was selected for in vivo pharmacology evaluation, and the result showed it has significant anti-tumor activity in the xenograft mouse models, demonstrating its potential utility in treatment of SqCC lung cancer.

2. Results and discussion

2.1. Hit identification and binding mode analysis

To identify the starting molecules for development, an in-house protein kinase inhibitor library containing 167 diversified molecules was subjected to DDR2 inhibition assay, and compound **1** with indazole scaffold was found to be a moderate inhibitor, showing enzymatic inhibition ratio about 76% at concentration of 20 μM. We performed the docking study to predict the binding mode of this hit compound with DDR2. Currently, there is no solved crystal structure of DDR2 deposited in PDB database, therefore homology modeling protocol was adopted, and the crystal structure of DDR1 (PDB entry 5FDP) was selected as template to build DDR2 model. Then Glide software was used for docking study, and the predicted binding conformation was depicted in Fig. 1A. From the docking prediction, compound **1** binds as a typical Type-II (DFG-out) kinase inhibitor, using the nitrogen atoms in indazole ring to form essential hydrogen bonds with hinge segment of DDR2. The amide group of compound **1** strengths the interactions by hydrogen bonding with the nearby residues Glu625 and Asp728(Fig. 1A), while the methyl pyridinone was situated at the hydrophobic sub-pocket near to the C-helix.

Type-II kinase inhibitors preferentially bind to the inactive conformation of the protein kinases, and requisitely interact with the hinge part that can contribute up to 40%–60% of the total binding free energy of the inhibitor. Therefore, this part is very essential for optimizing the activity of kinase inhibitors. Beside of the obvious H-bond interaction between the backbone nitrogen of Met657(Fig. 1A)and the N2 atom of indazole of compound **1**, there are two options of making further hydrogen bonding interaction with carbonyl oxygen atom of Asp702 or Met657. By surveying the reported type-II kinase inhibitors, we found that meta-CF_3 substituted benzene ring was usually employed to occupy the allosteric sub-pocket near the C-helix in the inactive conformation of kinase. Therefore, based on above-mentioned rationales, compounds **2**–**5** were synthesized to verify the predicted binding mode and to determine the scaffold for further optimization.

The bioactivities of compounds **2**–**5** were listed in Table 1. When the group N-(3-substituted)-3-(trifluoromethyl) benzamide was shifted from 5-position of indazole (**3**) to 6-position (**2**), activity was dramatically enhanced to moderate inhibitory rate at 100 nM. The bioactivity of compound with Methyl substituted on the nitrogen atom of indazole (**4**) was dramatically decreased, confirming that the NH of indazole played an important role in H-bond interaction with the hinge residues. Although an amine introduced to 3-position may participate in forming an additional hydrogen bonding with the hinge of kinase domain, however, as shown in Table 1, the compounds (**5** and **6**) displayed significantly reduced bioactivity when the amine group was attached to the indazole.

2.2. Optimizing the groups B and C

After the identification of proper hinge binder, the next step was to identify a proper linker between group A and group D. Refering to the reported type-II kinase inhibitors, Group C usually formed two and more H-bonds with a glutamic acid residue in the C-helix and an asparagic acid residue in the Asp-Phe-Gly (DFG) motif of

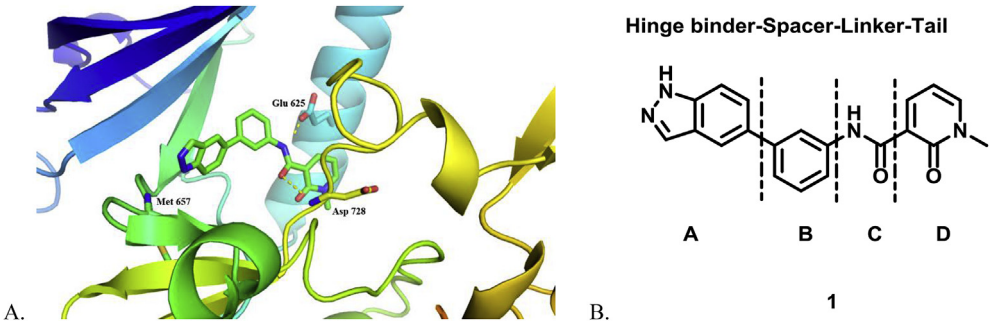

Fig. 1. A) Docking compound **1** into DDR2 kinase domain. And B) Optimizing four groups in SAR study based on the predicted binding mode. Group A, Hinge-binding Region. Group B, Linker between A and C. Group C, H-binding Region with Glu625 and Asp728. Group D, Tail in the allosteric region.

active loop of kinase domain. Amide and urea were typical functional groups to fulfill this H-bond capability. Therefore, amide and reversed amide were synthesized (**3** and **8,** Table 1) and the activities from the DDR2 enzyme assay showed no apparent difference. But when urea was applied to the molecule (**7**), a dramatic loss in activity indicated that the length of linker is critical for optimal interaction between the group D and the hydrophobic sub-pocket. Substituent on the benzene of group B always plays a critical role in the binding activity in Type II-kinase inhibitors. Therefore, methyl group was introduced at different positions to scan the position of "Flag Methyl". As shown in Table 2, methyl at R^1 position (**9a**) dramatically enhanced the enzymatic activity of DDR2, which indicated that this "Flag Methyl" was situated into a small hydrophobic cavity in the back pocket of DDR2 kinase. Further, different substituents were also applied at the R^1 position (**9e-9g**), and the result indicated that larger or smaller substituents such as methoxyl and fluorine had detrimental impact on binding interactions with this small hydrophobic cavity (see Table 3).

2.3. Exploration of the impact of group D on the binding

SAR study so far had led to compound **9a** as a basic skeleton because it showed a good potency towards DDR2 in the enzyme assay. Base on compound **9a**, exploration around group D was conducted to assess its impact on the binding activity. Firstly, trifluoromethyl was replaced by some lager hydrophobic group such as isopropyl and cyano substituted isopropyl (**10b** and **10c),** which showed similar bioactivities as **10a**. When methylene was inserted between the amide and benzene ring to change the chain length (**10d**), the activity of DDR2 was slightly decreased. Piperazine as a solubility-enhancing group was introduced into the molecules (**10e**-**10j**), resulting in an interesting SAR: direct substitution of trifluoromethyl with N-methyl piperazine (**10e**) sharply reduced the potency on DDR2; shifting the N-methyl piperazine to para-position (**10f**) showed similar inferior effects on bioactivity; extending the N-methyl piperazine by adding methylene (**10i**) to **10e** significantly enhanced the enzymatic activity on DDR2, which even amplified from the comparison of **10h** and **10f**; however, adding the piperazine motif to the molecules with longer linker **10g** showed diminished activity with respect to both **10i**. Based on the SAR study described above, trifluoromethyl and piperazine motifs were integrated into the molecules (**10j-10m**). As expected, these four compounds showed high potency on DDR2 enzymatic assay.

2.4. Improving the potency on FGFR1 and DDR2

Since FGFR1 also plays an important role in development of SqCC, we selected DDR2-potent compounds **10a-10c** and **10k-10n** to test the FGFR1 enzymatic inhibition. Generally, these compounds showed weak bioactivities in the FGFR1 enzymatic assay. To gain deep insight into the molecular basis on inhibitory activity, we analyzed the putative binding mode of compound **10a** with molecular docking with the binding site model of FGFR1 protein prepared from the PDB structure 4V04 (SI Fig. S3). From the docking prediction, the residue Tyr563 at the hinge segment drew our attention, as it might form a π-π stacking interaction if we introduce an aromatic ring at the 3-position of indazole, which will enhance the binding energy with the FGFR1 protein. Therefore, compound **11a** was synthesized to verify our assumption. As shown in Table 4, compound **11a** displayed significant potency not only in the FGFR1 and DDR2 enzymatic assays, but also in the cellular antiproliferative tests against the FGFR1-and DDR2-sensitive cell lines KG-1 and NCI-H2286 respectively. Following this, analogs (**11b-11e**) were prepared by adding different polar groups and showed similar activities in enzymatic assays. We selected compound **11a** to perform the primary mouse PK assessment, which resulting disappointed PK properties (Table 5). To solve this issue, an approach of replacing the benzene ring with a more druglike functional group pyrazole was adopted, producing compounds **11f-11r**. From the bioactivity tests, four compounds (**11g, 11h, 11k and 11r**) showed an obvious improvement on the activities.

2.5. In vivo PK study

Overall, considering the activity in enzymatic assays and cellular antiproliferative assays, four compounds **11g, 11k, 11m** and **11r** with different structural features were selected for in vivo pharmacokinetic assessment (CD-1 mice) to identify the best one for further evaluation. Among the selected compounds, **11k** exhibited excellent pharmacokinetic properties, with a good exposure ($AUC_{0-\infty}$ = 7636 ng*h/mL) and moderate half-life of 3.05 h. Incorporating previous optimization at Group D, we also prepared compound **12** by adding N-methyl piperazine to the tail of **11k** with the hope to further improve the solubility as well as the pharmacokinetic properties. From Table 6, although compound **12** has excellent inhibitory activities against FGFR1 and DDR2, it had much inferior PK parameters with respect to **11k**, especially the exposure parameter. To find the reason for this dramatic disparity, compound **11k** and **12** were subjected to Caco-2 monolayer permeability assay to assess the absorption issue. As shown in Table 6, although compound **12** had higher solubility, it proved to be a substrate of P-glycoprotein (P-gp) transporter with an efflux ratio more than 42 folds. Taking together, compound **11k** was selected for further study.

2.6. Kinase selectivity profile of 11k

The selectivity profile of compound **11k** was carried out over a

Table 1
SAR exploration of the hinge-binding region and group C[a].

Compd.	%@1000 nM	%@100 nM
	Inhibitory Rate (IR)	Inhibitory Rate (IR)
2	28.9%	14%
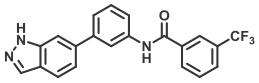		
3	90.8%	46.8%
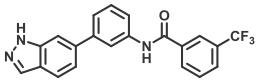		
4	29.8%	7.6%
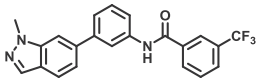		
5	35.9%	13.1%
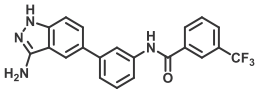		
6	24.8%	22.8%
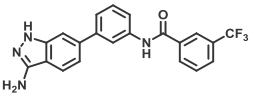		
7	53.3%	20.1%
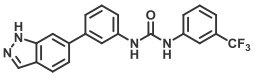		
8	84.7%	58.2%
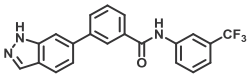		

Footnote.
[a] Inhibition ratio are given as the mean from two separate experiments. And the positive control compound Dasatinib has the IC_{50} value 1.4 ± 0.1 nM.

Table 2
SAR exploration of group B.[a]..

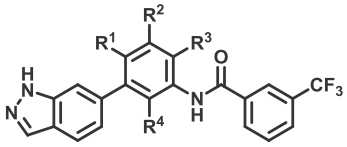

Compd.	R1	R2	R3	R4	DDR2 IC50 (nM)
9a	CH3	H	H	H	5.5 ± 0.5
9b	H	CH3	H	H	27.4%@ 100 nM[b]
9c	H	H	CH3	H	37.3%@ 100 nM
9d	H	H	H	CH3	41.8% @ 100 nM
9e	F	H	H	H	64.3 ± 0.6
9f	Cl	H	H	H	9.5 ± 1.3
9g	OCH3	H	H	H	67.9 ± 2.4

Footnote.
[a] IC_{50} values or inhibition ratios are calculated from two separate experiments. And the positive control compound Dasatinib has the IC_{50} value 1.4 ± 0.1 nM.
[b] Means the enzymatic inhibition rate at ligand concentration 100 nM.

panel of 30 kinases. As presented in Fig. 2, compound **11k** was clearly acting as a multi-target inhibitor, especially for the receptor tyrosine kinase subfamily, and showed high inhibitory activities towards VEGFR2 and EPH-B2. It also inhibited several kinases at moderate level, such as c-Src, CSF-1R, FLT-3, Abl, CDK6 and PDGFR-β. For the rest of tested kinases,it only showed high inhibition rate at 1 μM concentration. Although we only tested limited kinases, the data implied that **11k** has certain selectivity in the kinome.

2.7. Compound 11k blocks protein kinase phosphorylation and downstream signaling in cells

To investigate the kinase inhibitory activity against FGFR and DDR2 of compound **11k** at cellular level, both FGFR2-addicted cancer cell line SNU-16 cells and DDR2-dependent NCI-H2286 cells were tested. Firstly, we analyzed its' effects on the phosphorylation of FGFR and its key downstream signaling molecules Erk in SNU-16 cells. AZD4547,a selective FGFR1-3 inhibitor, was used as the positive control. **11k** showed significant inhibition of FGFR2 phosphorylation in a dose-dependent manner in SNU-16 cells. The phosphorylation of ERK was also unanimously inhibited (Fig. 3A). Thus, **11k** potently inhibits FGFR signaling activation. Similar result could be observed in NCI-H2286, a DDR2-dependent cell line with persistent activation of mutations in the DDR2 (I638F) site. DDR2 activates important signaling components such as ERK and PI3K/AKT [15,17]. We utilized multi-target inhibitor dasatinib as the positive control. **11k** showed significant inhibition of DDR2 phosphorylation in a dose-dependent manner in H2286 cells. The phosphorylation of AKT and ERK were also unanimously inhibited (Fig. 3B). All these data indicated that **11k** could block FGFR and DDR2 signaling at the cellular level.

2.8. Cellular antiproliferation activity

To further evaluated the impact of **11k** on FGFR and DDR2 overactivation-mediated cancer cell proliferation, five cancer cell lines harboring frequently occurring oncogenic forms of different FGFR members and DDR2 were chosen. As shown in Table 7, **11k** significantly inhibited the proliferation of FGFR-driven cancer cell lines with IC_{50} values of 108.4, 93.4, 31.8 and 306.6 against KG-1, SNU-16, NCI-H716 and UMUC14 respectively. Moreover, **11k** demonstrated substantially activity against the DDR2-driven

Table 3
SAR Exploration of Tail part.[a]..

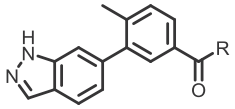

Compd.	R	DDR2 IC_{50} (nM)
10a		1.5 ± 0.1
10b		1.2 ± 0.2
10c		2.7 ± 0.3
10d		8.0 ± 0.2
10e		37.3%@100 nM[b]
10f		25.8%@100 nM
10g	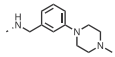	23.2%@100 nM
10h	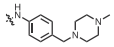	6.7 ± 0.5
10i	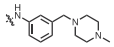	75.9 ± 7.6
10j		4.7 ± 0.8
10k		3.9 ± 0.7
10l	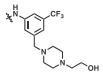	3.4 ± 0.1
10m		7.0 ± 0.2

Footnote.
[a] IC_{50} values or inhibition ratios are calculated from two separate experiments. And the positive control compound Dasatinib has the IC_{50} value 1.4 ± 0.1 nM.
[b] means the enzymatic inhibition rate at ligand concentration 100 nM.

cancer cell line NCI-H2286 (93.0 nM). Collectively, these results highlighted the antiproliferative activities of **11k** on FGFR-altered and DDR2-driven cancer cell lines.

2.9. In vivo antitumor efficacy in mouse models in SqCC

Classical FGFR-dependent NCI-H1581 lung cancer cell line-derived xenografts were first exploited to evaluate the vivo efficacy of compound **11k**. Nude mice bearing NCI-H1581 tumors were randomized and treated with compound **11k** at doses of 10 or 20 mg/kg daily consecutively. As shown in Fig. 4A, compound **11k**

Table 4
SAR Exploration of hinge part.[a]..

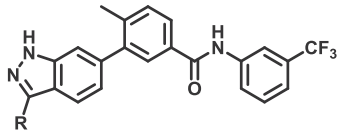

Compd.	R	FGFR1 IC_{50}(nM)	KG-1 IC_{50}(nM)	DDR2 IC_{50}(nM)	NCI-H2286 IC_{50}(nM)
11a		19.3 ± 10.7	136.4 ± 5.0	8.8 ± 0.9	89.5 ± 5.6
11b	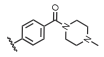	25.4 ± 5.5	300.3 ± 4.2	6.5 ± 0.2	45%@100 nM[b]
11c	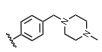	20.7 ± 4.8	119.5 ± 8.9	6.2 ± 0.2	13%@100 nM
11d		55.4 ± 32.0	561 ± 12.9	21.6 ± 2.1	140.4 ± 2.5
11e		9.0 ± 2.6	176.7 ± 4.8	8.7 ± 0.01	56%@1000 nM
11f		>100	>1000	55.6 ± 27.3	>1000
11g		6.4 ± 0.4	65.7 ± 12.9	4.4 ± 4.4	24.3 ± 2.5
11h		6.7 ± 1.0	257 ± 31.1	2.6 ± 1.7	19.8 ± 0.01
11i		12.9 ± 2.6	358 ± 38.7	3.2 ± 0.8	41%@100 nM
11j		20.1 ± 8.8	452 ± 10.7	7.7 ± 0.7	31%@100 nM
11k		31.1 ± 3.3	108.4 ± 2.1	3.2 ± 0.2	93.0 ± 8.7
11l		11.6 ± 1.1	173.6 ± 11.5	2.9 ± 0.1	35%@100 nM
11m		26.8 ± 4.7	339 ± 29.5	3.7 ± 0.01	196.2 ± 12.7
11n		11.7 ± 0.7	441 ± 23.8	2.7 ± 0.1	>1000
11o		11.5 ± 0.6	114.±16.4	2.6 ± 0.3	49%100 nM
11p		6.7 ± 1.1	303.6 ± 1.8	6.2 ± 0.1	69.7 ± 0.4
11q		3.2 ± 0.1	121.1 ± 1.2	5.2 ± 0.2	45%@100 nM
11r		10.1 ± 2.7	93.3 ± 4.3	3.8 ± 0.4	56.5 ± 5.3

Footnote.
[a] IC_{50} values or inhibition ratios are calculated from two separate experiments. And the positive control compound Dasatinib has the IC_{50} value 1.4 ± 0.1 nM towards DDR2, while the positive control compound AZD4547 has the IC_{50} value 1.1 ± 0.4 nM towards FRFR1.
[b] means the enzymatic inhibition rate at ligand concentration 100 nM.

could suppress tumor growth in a dose-dependent manner with tumor growth inhibition rates (TGI) of 59.7% and 98.1% at doses of 10 and 20 mg/kg, respectively, indicating that compound **11k** has profound anti-tumor efficacy in NCI-H1581 tumor model. Although over 200 cell lines for NSCLC have been reported, only about 30 are SqCC cell lines and even among these, some have been erroneously categorized and are in fact poorly differentiated carcinomas [19]. Development of pre-clinical mouse models for SqCC has lagged far behind due to the lack of validated driver mutations, unclear cell or origin and difficulty replicating the complex genomic landscape of the disease [20]. So we develop NCI-H2286 SCID mouse model for SqCC. SCID mice bearing NCI-H2286 tumors were randomized and treated with compound **11k** at doses of 10 mg/kg for 10 consecutive days. As shown in Fig. 4B, compound **11k** could suppress tumor growth with tumor growth inhibition rates (TGI) of 82.8%. Dasatinib in the positive control group suppressed tumor growth with tumor growth inhibition rates (TGI) of 50.9% at doses of 50 mg/kg, demonstrating that compound **11k** elicited marked anti-tumor efficacy in NCI-H2286 tumor model. Although compound **11k** showed less potent than AZD4547 and Dasatinib at blocking the phosphorylation of FGFR2 and DDR2 in western blot experiment (Fig. 3), **11k** showed better tumor suppression effects in vivo, which could be due to the fact that **11k** acted as a multi-target inhibitor, while AZD4547 only selectively targets the FGFRs and dasatinib has very weak inhibitory activity to FGFRs. Another possible reason of better efficacy may stems from the good pharmacokinetics of compound 11k, although we did not directed compare with the PK profiles of two positive control compounds.

Table 5
Pharmacokinetics Profiles of compound 11a, 11g, 11k, 11 m,11r and 12.

Compd.	dosage	$T_{1/2}$	T_{max}	C_{max}	AUC_{0-t}	$AUC_{0-\infty}$	MRT
	mg/kg (po)	h	h	(ng/ml)	(h*ng/ml)	(h*ng/ml)	h
11a	10	–	1.33	15.9	44.0	–	–
11g	10	2.75	1.17	890	3475	3485	3.26
11k	10	3.05	2.00	1125	7636	7680	5.71
11m	10	0.75	0.25	202	324	334	1.37
11r	10	2.75	1.33	170	552	563	3.96
12	10	1.4	1.67	111.2	66.2	610.10	3.2

Table 6
Compound 11k and 12 and the Caco-2 monolayer permeability assay of 11k and 12.

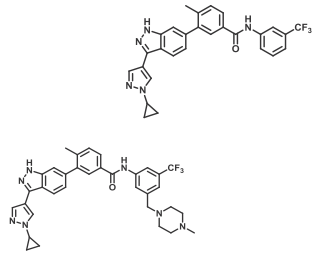

Compound	11k	12
DDR2	3.2 ± 0.2 nM	5.7 ± 1.4 nM
Minimal Soluble Concentration	2 μM	10 μM
Permeability (Mean Fabs)	48.6%	12.0%
Efflux Ratio	1.1	42.7

2.10. Primary assessment of drug-likeness of compound *11k*

To further evaluate compound **11k** as a potential candidate, herein, we examined it in vitro drug metabolism by using a standard human and rat microsomal stability assay. The results indicated compound **11k** was very stable in the human and rat liver microsomes (Table 8). As cytochrome P450s (CYPs) are the major enzymes involved in the metabolism of various xenobiotics, we selected five human hepatic CYP enzymes that play a dominant role in the metabolism of drugs and other xenobiotics to investigate the risk of drug-drug interaction. As shown in Table 8, compound **11k** had very weak inhibitory activities against the most relevant 3A4 and 2D6, but showed moderate inhibition towards 2C9 and 2C19 subtypes. Since 3A family is responsible for metabolism of about 50% of drugs and 2D6 is responsible for metabolism of about 30% of drugs [21], we thought compound **11k** poses lower risk in drug-drug interactions. We also checked the time-dependent inhibition (TDI) of **11k**, which is to study the irreversible inhibition of the compound. If TDI happens, it will take several days for the CYP enzymes to be regenerated, which will pose serious issues for drug elimination. Luckily, according to the result in Table 8, no TDI inhibition against the five CYP enzymes was found, even for 2C9 and 2C19. This further reinforced that compound **11k** may have lower risk in drug-drug interaction.

In recent days, hERG inhibition brought the concern about heart toxicity, as it may affect the cardiac action potential. This made hERG inhibitory assay a necessity for candidate evaluation.

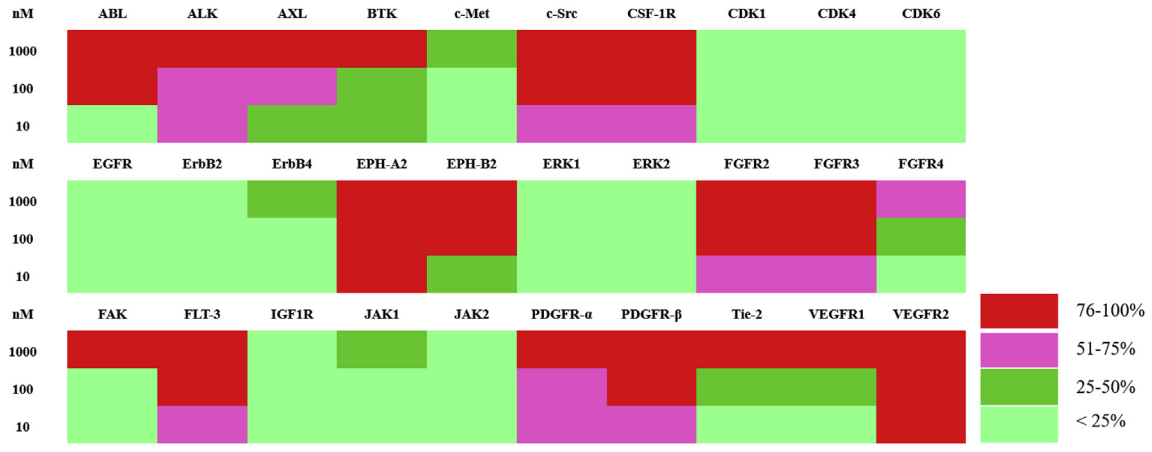

Fig. 2. In vitro enzymatic screen assays of compound 11k.

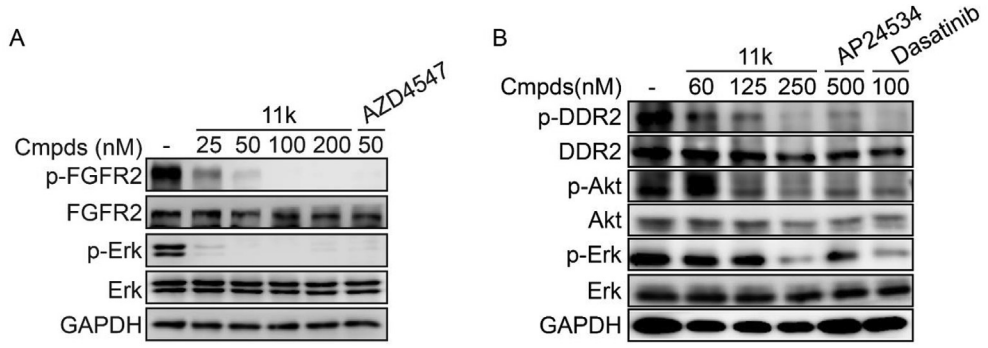

Fig. 3. Compound 11k blocks tyrosine kinase phosphorylation and downstream signaling in cells. Cells including SNU-16 (A), NCI-H2286 (B) treated with 11k for 2 h at the indicated concentrations were lysed and subjected to Western blot analysis.

Table 7
The anti-proliferative effects of **11k** against related cell lines.

Cell lines		IC50 (nM)[a]		
		11k	AZD4547	Dasatinib
KG-1	FGFR1 fusion	108.4 ± 2.1	5.8 ± 0.6	/
SNU-16	FGFR2 amplification	93.4 ± 0.9	19.6 ± 0.5	/
NCI-H716	FGFR2 amplification	31.8 ± 8.8	5.9 ± 2.1	/
UMUC14	FGFR3 mutation	306.6 ± 48.3	4.5 ± 0.1	/
NCI-H2286	DDR2 mutation	93.0 ± 8.7	/	33.3 ± 6.3

Footnote.
[a] Values are the mean ± SD of two independent assays.

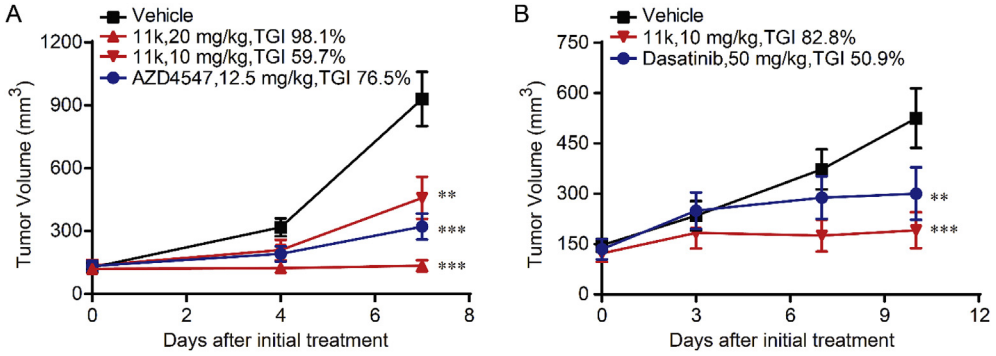

Fig. 4. A) Compound **11k** inhibits tumor growth in NCI-H1581 xenografts. Mice were randomly assigned to control vehicle and treatment groups (n = 6 in treated group, n = 12 in vehicle group) when the tumor volume reached 100–150 mm^3. The control groups were given vehicle alone, and the treatment groups received **11k** and AZD4547 at the indicated doses via oral administration once daily for 7 days. B) Compound **11k** inhibits tumor growth in NCI-H2286 xenografts. Mice were randomly assigned to control vehicle and treatment groups (n = 5 in treated group, n = 10 in vehicle group) when the tumor volume reached 100–150 mm^3. The control groups were given vehicle alone, and the treatment groups received **11k** and Dasatinib at the indicated doses via oral administration once daily for 10 days. The results are expressed as the mean ± SEM with $^{**}p < 0.01$, and $^{***}p < 0.001$ vs control group determined using Student's *t*-test. The Tumor Volume was measured on the final day of the study for the drug-treated mice compared with the control mice.

Compound **11k** did not show an evident inhibitory effect on hERG, with an IC_{50} of more than 40 μM from an automated patch clamp electrophysiology measurement (Fig. S4 in SI.). Taken together these druglike assessments, compound **11k** showed promise as a drug candidate for further development.

3. Chemistry

Starting from aniline (**13**) or carboxylic acid (**16**), the corresponding boronate ester intermediate (**14,15,17**) was obtained by condensation with carboxylic acid, isocyanate or amine,and then coupled with the corresponding halogenated aromatic ring to obtain compound **2**–**8** via Suzuki-Miyaura reaction (Scheme 1). In Scheme 2, different substituted anilines were condensed with 3-(trifluoromethyl) benzoic acid in DMF under the conditions of HATU as a condensing agent to obtain the corresponding intermediate **19a-g**, which underwent another coupling to yield desired compounds **9a-g**. Compounds **10a-i** in Scheme 3 were also obtained by condensation reaction and Suzuki coupling reaction as above. The active ester solution formed by 3-bromo-4-methylbenzoic acid and HATU slowly added dropwise to a dilute solution of 3-amino-5-(trifluoromethyl)phenyl) methanol under low temperature, thereby obtaining intermediate **23**, and then benzyl bromide intermediate **24** is obtained by Appel reaction with triphenylphosphine and NBS. N-substituted piperazine via substituting with compound **24** to obtain intermediates **25j-m**, and by Suzuki coupling reaction to obtain final product **10j-10m**. The intermediates **27a**–**r** could be obtained by the coupling of 6-

Table 8
Compound 11k In vitro liver microsome stability test.

HLM Stability Clint(ul/min/mg protein)		MLM Stability Clint(ul/min/mg protein)	
0		0	
Reversible CYP Inhibition of 11k (Direct Inhibition Mean,DI)[a]		Irreversible CYP Inhibition of 11k (Time Dependent Inhibition, TDI)[b]	
3A4-MDZ	16%	3A4-MDZ	90
3A4-Testo	5%	3A4-Testo	100
2D6	10%	2D6	70
2C9	83%	2C9	100
1A2	20%	1A2	110
2C19	64%	2C19	90

Footnote.
[a] DI<20% No Inhibition; 20% < DI<50% Weak Inhibition; 50% < DI<70% Moderate Inhibition; DI >70% Strong Inhibition.
[b] TDI>200 will be considered as irreversible CYP Inhibition.

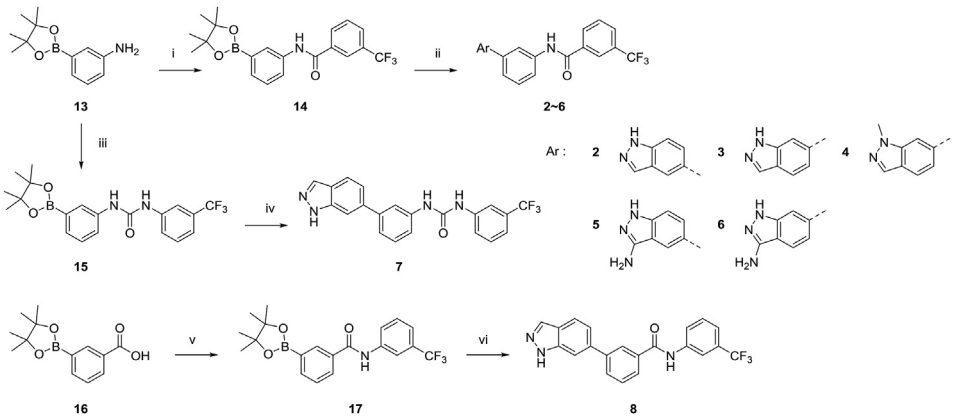

Scheme 1. Synthesis route of compounds 2–8. [a]Reagents and conditions: (i) 3-(trifluoromethyl) benzoic acid, HATU, DIPEA, DMF, 25 °C; (ii) Aromatic halide, $Pd(dppf)_2Cl_2 \cdot CH_2Cl_2$, K_2CO_3, 1,4-dioxane, H_2O, 80 °C; (iii) 1-isocyanato-3-(trifluoromethyl) benzene, THF, 25 °C; (iv) 6-bromo-1H-indazole, $Pd(dppf)_2Cl_2 \cdot CH_2Cl_2$, K_2CO_3,1,4-dioxane, H_2O, 80 °C; (v) thionyl chloride, 80 °C, refflux; then 3-(trifluoromethyl) aniline, DIPEA, THF, 0 °C (vi) 6-bromo-1H-indazole, $Pd(dppf)_2Cl_2 \cdot CH_2Cl_2$, K_2CO_3, 1,4-dioxane, H_2O, 80 °C;

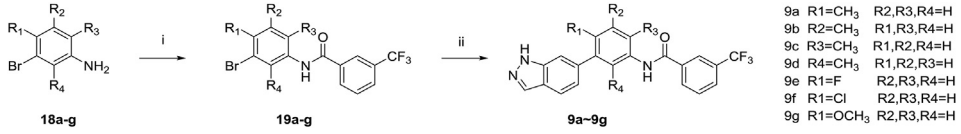

Scheme 2. The synthesis route of compounds 9a-9g. [a]Reagents and conditions: (i) 3-(trifluoromethyl) benzoic acid, HATU, DIPEA, DMF, 25 °C; (ii) 6-(4,4,5,5-tetramethyl-1,3,2-dioxaborolan-2-yl)-1H-indazole $Pd(dppf)_2Cl_2 \cdot CH_2Cl_2$, K_2CO_3, 1,4-dioxane, H_2O,80 °C;

bromo-3-iodo-1H-indazole with different phenyl boronates or boronic acids at 1:1 equivalent. The following step Suzuki coupling of **27a-r** with intermediate **21a** afforded desired compounds **11a-11r** (Scheme 3). Boronic ester **28** were provided from **25k** via a Miyaura borylation reaction. The coupling of **28** and **27k** provided desired compound **12** (see Scheme 4).

4. Conclusion

In summary, a novel series of 3-position substituted indazole derivatives were designed, synthesized, and evaluated as multi-target kinase inhibitors for the treatment of SqCC. The hit compound was identified from an in-house kinase library. On the basis of homology modeling and docking, we identified it to be a type II inhibitor, and subjected for SAR explorationby deviding it into four parts of Hinge binder, Spacer, Linker and Cap part. Among them, compound **11k** showed high potency against FGFR1 and DDR2 kinase with good DMPK (Drug Metabolism and Pharmacokinetics) properties. Furthermore, in vivo pharmacology evaluations of compound **11k** showed significant antitumor activity (TGI = 90.92%) in FGFR-driven NCI-H1581 xenograft model and (TGI = 89.00%) DDR2-driven NCI-H2286 xenograft model. These imply that compound **11k** deserves further research.

Previous clinical studies on molecular targeted agents in SqCC have unfortunately been negative, such as trials involving kinase inhibitors sorafenib, motesanib, cediranib or iniparib. Squamous cell lung cancer has long been considered a challenging tumor type to treat, at least partly due to the lack of clear driver mutations. Therefore, many questions remain to be solved, such as: Is the DDR2 mutation concomitant with the appearance of FGFR1 amplification, and/or PI3KCA mutations? Does the multi-target strategy provide enough safety windows for treatment? Is there a representative SqCC mouse model can be used for drug discovery? We hope that compounds discovered in present study could stimulate further study on SqCC drug development.

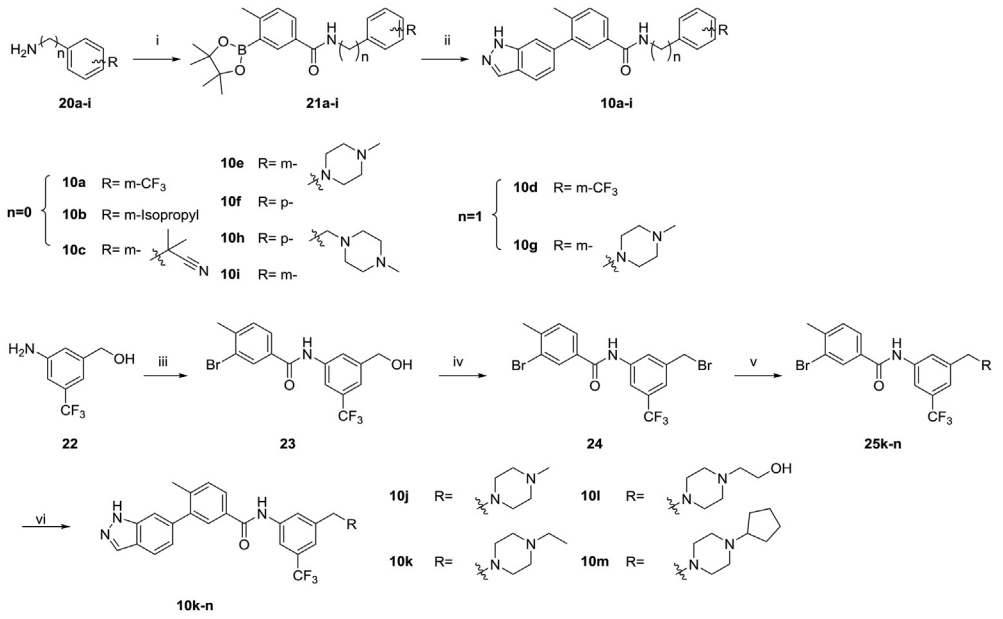

Scheme 3. The synthesis route of compounds 10a-m. [a]Reagents and conditions: (i) 4-methyl-3-(4,4,5,5-tetramethyl-1,3,2-dioxaborolan-2-yl) benzoic acid, HATU, DIPEA, DMF, 25 °C; (ii) 6-bromo-1H-indazole, $Pd(dppf)_2Cl_2 \cdot CH_2Cl_2$, K_2CO_3, 1,4-dioxane, H_2O, 80 °C; (iii) 3-bromo-4-methylbenzoic acid, HATU, DIPEA, DMF, 25 °C; (iv) triphenylphosphine, N-Bromosuccinimide, Toluene, 0–25 °C(v) N-substituted piperazine, DIPEA, DCM, 25 °C; (vi) 6-(4,4,5,5-tetramethyl-1,3,2-dioxaborolan-2-yl)-1H-indazole, $Pd(dppf)_2Cl_2 \cdot CH_2Cl_2$, K_2CO_3, 1,4-dioxane, H_2O, 80 °C;

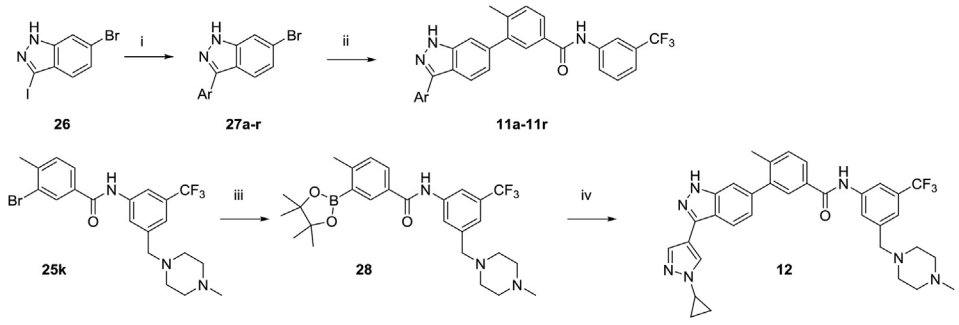

Scheme 4. The synthesis route of compounds 11a-11r and 12. [a]Reagents and conditions: (i) Aromatic boric acid(esters), $Pd(dppf)_2Cl_2 \cdot CH_2Cl_2$, K_2CO_3, 1,4-dioxane, H_2O, 80 °C; (ii) **21a**, $Pd(dppf)_2Cl_2 \cdot CH_2Cl_2$, K_2CO_3, 1,4-dioxane, H_2O, 80 °C; (iii) Bis(pinacolato)diboron, $Pd(dppf)_2Cl_2 \cdot CH_2Cl_2$, AcOK, DMSO, 80 °C; (iv) **27k**, $Pd(dppf)_2Cl_2 \cdot CH_2Cl_2$, K_2CO_3, 1,4-dioxane, H_2O, 80 °C;

5. Experimental section

5.1. Chemistry

5.1.1. General

^1H NMR (400 MHz) spectra were recorded with a Varian Mercury-400 High Performance Digital FT-NMR spectrometer with tetramethylsilane (TMS) as an internal standard. ^{13}C NMR (100 MHz or 125 MHz or 151 MHz) spectra were recorded by using a Varian Mercury-400 High Performance Digital FT-NMR spectrometer or Varian Mercury-500 High Performance Digital FT-NMR spectrometer or Varian Mercury-600 High Performance Digital FT-NMR spectrometer. Abbreviations for peak patterns in NMR spectra: br = broad, s = singlet, d = doublet, and m = multiplet. Low-resolution mass spectra were obtained with a Finnigan LCQ Deca XP mass spectrometer using a CAPCELL PAK C18 (50 mm × 2.0 mm,5 μM) or an Agilent ZORBAX Eclipse XDB C18 (50 mm × 2.1 mm,5 μM) in positive or negative electrospray mode. Low-resolution mass spectra and high-resolution mass spectra were recorded at an ionizing voltage of 70eV on a Finnigan/MAT95 spectrometer. High-resolution mass spectra were recorded by using a Finnigan MAT-95 mass spectrometer or an Agilent technologies 6224 TOF mass spectrometer. Purity of all compounds was determined by analytical Gilson high-performance liquid chromatography (HPLC) using an YMC ODS3 column (50 mm × 4.6 mm, 5 μM). Conditions were as follows: CH_3CN/H_2O eluent at 2.5 mL min^{-1} flow [containing 0.1% trifluoroacetic acid (TFA)] at 35 °C, 8min, gradient 5% CH_3CN to 95% CH_3CN, monitored by UV absorption at 214 nm and 254 nm. TLC analysis was carried out with glass precoated silica gel GF254 plates. TLC spots were visualized under UV light. Flash column chromatography was performed with a Teledyne ISCO CombiFlash Rf system. All solvents and reagents were used directly as obtained commercially unless otherwise noted. Anhydrous dimethylformamide was purchased from Acros and was used without further drying. All air and moisture sensitive reactions were carried out under an atmosphere of dry Argon with heat-dried glassware and standard syringe techniques.

5.1.2. Synthetic procedures

*5.1.2.1. N-(3-(4,4,5,5-tetramethyl-1,3,2-dioxaborolan-2-yl)phenyl)-3-(trifluoromethyl)benzamide(**14**).* 3-(trifluoromethyl) benzoic acid

(4.4g, 22.82 mmol) was stirred in a solvent of dimethyl formamide (15 mL). The reaction solution was added with HATU (9.55 g, 25.10 mmol), DIPEA (7.54 mL, 45.64 mmol) and 3-(4,4,5,5-tetramethyl-1,3,2-dioxaborolan-2-yl) aniline (5.00 g, 22.82 mmol, **13**), followed by stirring for about 6 h at room temperature. The reaction mixture was diluted with ethyl acetate and washed with a saturated aqueous sodium bicarbonate solution and saline. The organic layer thus obtained was dried over anhydrous sodium sulfate, filtered, and concentrated under reduced pressure. The resulting mixture was concentrated to give the crude product, which was purified by silica gel column chromatography (eluting with 0–5% EtOAc in petroleum ether) to provide **14** as a white solid (7.5 g, 84%).^{1}H NMR (400 MHz, Methanol-d4) δ 8.29 (s, 1H), 8.23 (d, J = 8.0 Hz, 1H), 8.07 (s, 1H), 7.91 (d, J = 7.6 Hz, 1H), 7.86 (d, J = 8.3 Hz, 1H), 7.75 (t, J = 7.9 Hz, 1H), 7.57 (d, J = 7.3 Hz, 1H), 7.41 (t, J = 7.7 Hz, 1H), 1.38 (s, 12H). MS m/z: 392.1 ([M+H] $^+$).

*5.1.3. General procedure for the preparation of compounds **2,3,4,5,6***

*5.1.3.1. N-(3-(1H-indazol-5-yl)phenyl)-3-(trifluoromethyl)benzamide (**2**).* To a resealable vial was added K_2CO_3 (112 mg, 0.81 mmol), **14** (160 mg, 0.41 mmol), 5-bromo-1H-indazole (80 mg, 0.41 mmol). The vial was sealed and evacuated and purged with Ar for 5 min before addition of $PdCl_2$(dppf)-CH_2Cl_2 Adduct (20 mg, 0.02 mmol), dissolved in 1,4-dioxane/water (10 mL, 4:1, v/v) was then added to this solution before the vial was heated to 80 °C overnight. The reaction was cooled to room temperature, which was then brought to basic using aqueous sodium bicarbonate solution and extracted with ethyl acetate. The organic layer was collected and distilled under reduced pressure. The crude residue was purified via by silica gel column chromatography (eluting with 0–20% EtOAc in petroleum ether) to afford **2** as a white solid (85 mg, 55%). ^{1}H NMR (400 MHz, Methanol-d_4) δ 8.32 (s, 1H), 8.27 (d, J = 7.7 Hz, 1H), 8.14 (s, 1H), 8.09 (s, 1H), 8.06 (s, 1H), 7.93 (d, J = 7.6 Hz, 1H), 7.80–7.73 (m, 2H), 7.72 (d, J = 7.1 Hz, 1H), 7.65 (d, J = 8.7 Hz, 1H), 7.54–7.50 (m, 1H), 7.48 (d, J = 7.7 Hz, 1H). ^{13}C NMR (126 MHz, DMSO-d_6) δ 164.53, 141.80, 139.90, 139.80, 136.23, 134.49, 133.06, 132.32, 130.24, 129.73, 129.67 (d, J = 32.1 Hz), 128.66, 126.00, 124.70, 124.46 (d, J = 272.4 Hz), 124.01, 122.98, 119.50, 119.32, 118.70, 111.09. HRMS m/z (ESI) found 382.116 (M + H)$^+$, $C_{21}H_{15}F_3N_3O^+$ calcd for 382.1162, retention time 3.62 min, >99% pure.

*5.1.4. Compound **3,4,5,6** was prepared with a similar procedure as that used for **2***

*5.1.4.1. N-(3-(1H-indazol-6-yl)phenyl)-3-(trifluoromethyl)benzamide (**3**).* White solid, Yield: 63%. ^{1}H NMR (400 MHz, Methanol-d_4) δ 8.32 (s, 1H), 8.26 (d, J = 8.0 Hz, 1H), 8.14 (s, 1H), 8.09 (s, 1H), 7.93 (d, J = 7.8 Hz, 1H), 7.87 (dd, J = 8.5, 0.7 Hz, 1H), 7.79 (s, 1H), 7.78–7.72 (m, 2H), 7.54–7.52 (m, 1H), 7.50 (s, 1H), 7.48 (d, J = 1.4 Hz, 1H). ^{13}C NMR (126 MHz, DMSO-d_6) δ 164.58, 141.59, 141.00, 139.86, 138.59, 136.21, 133.90, 132.34, 130.24, 129.81, 129.68 (d, J = 32.1 Hz), 128.67, 124.72, 124.46 (d, J = 272.7 Hz), 123.27, 122.78, 121.53, 120.43, 119.91, 119.72, 108.05.HRMS m/z (ESI) found 382.1164 (M + H)$^+$, $C_{21}H_{15}F_3N_3O^+$ calcd for 382.1162, retention time 3.45 min, >99% pure.

*5.1.4.2. N-(3-(1-methyl-1H-indazol-6-yl)phenyl)-3-(trifluoromethyl) benzamide (**4**).* White solid, Yield: 47%. ^{1}H NMR (400 MHz, Methanol-d_4) δ 8.33 (s, 1H), 8.27 (d, J = 7.9 Hz, 1H), 8.16 (s, 1H), 8.04 (s, 1H), 7.93 (d, J = 8.4 Hz, 1H), 7.85 (d, J = 8.4 Hz, 1H), 7.81 (s, 1H), 7.73–7.80 (m, 2H), 7.58 (d, J = 7.9 Hz, 1H), 7.49–7.54 (m, 2H), 4.14 (s, 3H). ^{13}C NMR (126 MHz, Methanol-d4) δ 165.71, 141.95, 140.51, 139.70, 138.77, 135.84, 132.21, 130.94, 130.62 (d, J = 32.6 Hz), 129.25, 128.99, 128.98 (q, J = 3.5 Hz), 124.17 (q, J = 4.1 Hz), 123.97 (d, J = 271.5 Hz), 123.58, 123.14, 121.02, 120.53, 120.02, 119.95, 106.94, 34.16.HRMS m/z (ESI) found 396.1311 (M + H)$^+$, $C_{22}H_{17}F_3N_3O^+$ calcd for 396.1318, retention time 3.92 min, >99% pure.

*5.1.4.3. N-(3-(3-amino-1H-indazol-5-yl)phenyl)-3-(trifluoromethyl) benzamide (**5**).* White solid, Yield: 73%. ^{1}H NMR (400 MHz, Methanol-d_4) δ 8.31 (s, 1H), 8.24 (d, J = 7.9 Hz, 1H), 8.07 (s, 1H), 7.99 (s, 1H), 7.94–7.87 (m, 1H), 7.74 (q, J = 7.4 Hz, 1H), 7.7–7.62 (m, 2H), 7.51–7.43 (m, 2H), 7.39 (dd, J = 8.6, 2.7 Hz, 1H). ^{13}C NMR (126 MHz, DMSO-d_6) δ 164.50, 150.15, 142.19, 141.44, 139.76, 136.23, 132.31, 130.26, 130.23, 129.68 (d, J = 32.0 Hz), 129.61, 128.63, 125.95, 124.69 (d, J = 4.2 Hz), 124.46 (d, J = 272.6 Hz), 122.69, 119.23, 119.00, 118.80, 115.20, 110.34. HRMS m/z (ESI) found 397.1285 (M + H)$^+$, $C_{21}H_{16}F_3N_4O^+$ calcd for 397.1271, retention time 3.10 min, >99% pure.

*5.1.4.4. N-(3-(3-amino-1H-indazol-6-yl)phenyl)-3-(trifluoromethyl) benzamide (**6**).* White solid, Yield: 73%. ^{1}H NMR (400 MHz, Methanol-d_4) δ 8.32 (s, 1H), 8.26 (d, J = 7.8 Hz, 1H), 8.10 (d, J = 2.2 Hz, 1H), 7.93 (d, J = 7.6 Hz, 1H), 7.81–7.70 (m, 3H), 7.55 (s, 1H), 7.52–7.48 (m, 2H), 7.33 (d, J = 8.4,1H). ^{13}C NMR (126 MHz, DMSO-d_6) δ 164.55, 149.60, 142.58, 141.91, 139.79, 138.72, 136.22, 132.33, 130.23, 129.71, 129.67 (d, J = 32.0 Hz), 128.66 (q, J = 3.9 Hz), 124.70 (q, J = 4.1 Hz), 124.46 (d, J = 272.5 Hz), 123.16, 121.30, 119.75, 119.62, 117.49, 113.99, 107.50. HRMS m/z (ESI) found 397.1276 (M + H)$^+$, $C_{21}H_{16}F_3N_4O^+$ calcd for 397.1271, retention time 2.94 min, >98% pure.

*5.1.4.5. 1-(3-(4,4,5,5-tetramethyl-1,3,2-dioxaborolan-2-yl)phenyl)-3-(3-(trifluoromethyl)phenyl)urea(**15**).* The 3-(4,4,5,5-tetramethyl-1,3,2-dioxaborolan-2-yl) aniline (200 mg, 0.91 mmol). in 50 ml of dry tetrahydrofuran was added dropwise to the 1-isocyanato-3-(trifluoromethyl) benzene (172 mg, 0.91 mmol) at 0 °C with stirring. The ice-bath was removed after the completion of addition of the isocyanate and the mixture was stirred at room temperature for 4 h. The precipitate formed was isolated via filtration. The product as a white solid (350 mg, 94%) was dried in vacuo and carried forward to the next step without further purification. ^{1}H NMR (400 MHz, DMSO-d_6) δ 9.03 (s, 1H), 8.83 (s, 1H), 8.01 (s, 1H), 7.87 (d, J = 2.4 Hz, 1H), 7.57 (t, J = 8.3, 1.5 Hz, 1H), 7.54–7.46 (m, 2H), 7.35–7.27 (m, 3H), 1.29 (s, 12H). MS m/z: 407.3 ([M+H]$^+$).

*5.1.4.6. 1-(3-(4,4,5,5-tetramethyl-1,3,2-dioxaborolan-2-yl)phenyl)-3-(3-(trifluoromethyl)phenyl)urea (**7**).* To a resealable vial was added K_2CO_3 (112 mg, 0.81 mmol), **15** (181 mg, 0.45 mmol), 6-bromo-1H-indazole (80 mg, 0.41 mmol). The vial was sealed and evacuated and purged with Ar for 5 min before addition of $PdCl_2$(dppf)-CH_2Cl_2 Adduct (20 mg, 0.02 mmol), dissolved in 1,4-dioxane/water (10 mL, 4:1, v/v) was then added to this solution before the vial was heated to 80 °C overnight. The reaction was cooled to room temperature, which was then brought to basic using aqueous sodium bicarbonate solution and extracted with ethyl acetate. The organic layer was collected and distilled under reduced pressure. The crude residue was purified via by silica gel column chromatography (eluting with 0–30% EtOAc in petroleum ether) to afford the product as a white solid (92 mg, 57%). ^{1}H NMR (400 MHz, Methanol-d_4) δ 8.08 (s, 1H), 7.96 (s, 1H), 7.90 (s, 1H), 7.86 (d, J = 8.4 Hz, 1H), 7.78 (s, 1H), 7.64 (d, J = 8.2 Hz, 1H), 7.58–7.45 (m, 2H), 7.42 (m, 3H), 7.32 (d, J = 7.8 Hz, 1H). HRMS m/z (ESI) found 397.1273 (M + H)$^+$, $C_{21}H_{16}F_3N_4O^+$ calcd for 397.1271, >98% pure.

*5.1.4.7. 3-(4,4,5,5-Tetramethyl-1,3,2-dioxaborolan-2-yl)-N-(3-(trifluoromethyl)phenyl)benzamide (**17**).*

3-(4,4,5,5-tetramethyl-1,3,2-dioxaborolan-2-yl)benzoic acid (300 mg, 1.21 mmol, **16**) was dissolved in thionyl chloride (3 mL) and a catalytic amount of DMF were added, and the mixture was stirred at 78 °C for 3 h. The reaction mixture was concentrated under reduced pressure to give acid chloride. The acid chloride was

dissolved in THF (5 mL), 3-(trifluoromethyl) aniline (195 mg, 1.21 mmol) and DIPEA (0.400 mL, 2.42 mmol) were added, and the mixture was stirred at room temperature for 5 h. The reaction mixture was diluted with ethyl acetate and washed with brine. The organic layer was evaporated under reduced pressure and the obtained crude product was purified via by silica gel column chromatography (eluting with 0–10% EtOAc in petroleum ether) to afford the product as a white solid (350 mg, 74%). ^{1}H NMR (400 MHz, DMSO-d_6) δ 10.66 (s, 1H), 8.26 (d, J = 13.3, 1.7 Hz, 2H), 8.10 (ddd, J = 8.4, 4.9, 3.3 Hz, 2H), 7.90 (dt, J = 7.3, 1.2 Hz, 1H), 7.59 (dt, J = 11.1, 7.8 Hz, 2H), 7.51–7.41 (m, 1H), 1.33 (s, 12H). MS m/z: 392.3 ([M+H]$^+$).

*5.1.4.8. 3-(1H-indazol-6-yl)-N-(3-(trifluoromethyl)phenyl)benzamide (**8**).* To a resealable vial was added K_2CO_3 (112 mg, 0.81 mmol), **17** (175 mg, 0.45 mmol), 6-bromo-1H-indazole (80.0 mg, 0.41 mmol). The vial was sealed and evacuated and purged with Ar for 5 min before addition of $PdCl_2$(dppf)-CH_2Cl_2 Adduct (20 mg, 0.02 mmol), dissolved in 1,4-dioxane/water (10 mL, 4:1, v/v) was then added to this solution before the vial was heated to 80 °C overnight. The reaction was cooled to room temperature, which was then brought to basic using aqueous sodium bicarbonate solution and extracted with ethyl acetate. The organic layer was collected and distilled under reduced pressure. The crude residue was purified via by silica gel column chromatography (eluting with 0–30% EtOAc in petroleum ether) to afford the product as a white solid (96 mg, 62%). ^{1}H NMR (400 MHz, Methanol-d_4) δ 8.31 (s, 1H), 8.22 (s, 1H), 8.10 (s, 1H), 8.02–7.94 (m, 3H), 7.90 (d, J = 8.4 Hz, 1H), 7.86 (s, 1H), 7.66 (t, J = 7.8 Hz, 1H), 7.59 (d, J = 7.9 Hz, 1H), 7.58–7.52 (m, 1H), 7.46 (d, J = 7.8 Hz, 1H). ^{13}C NMR (126 MHz, DMSO-d_6) δ 166.31, 141.31, 140.98, 140.43, 137.95, 135.58, 133.94, 131.04, 130.36, 129.98, 129.72, 127.35, 126.80, 124.64 (d, J = 272.2 Hz), 124.30, 122.91, 121.61, 120.60, 120.48, 116.92, 108.51.HRMS m/z (ESI) found 382.1168 (M + H)$^+$, $C_{21}H_{15}F_3N_3O^+$ calcd for 382.1162, retention time 3.76 min, >97% pure.

*5.1.5. General procedure for the preparation of compounds **19a-g***

*5.1.5.1. N-(3-bromo-4-methylphenyl)-3-(trifluoromethyl)benzamide (**19a**).* 3-(trifluoromethyl) benzoic acid (511 mg, 2.69 mmol) was stirred in a solvent of dimethyl formamide (10 mL).The reaction solution was added with HATU (1.12 g, 2.96 mmol), DIPEA (890 μl, 5.37 mmol) and the appropriate substituted aromatic amine (500 mg, 2.69 mmol), followed by stirring for about 8 h at room temperature. The reaction mixture was diluted with ethyl acetate and washed with a saturated aqueous sodium bicarbonate solution and saline. The organic layer thus obtained was dried over anhydrous sodium sulfate, filtered, and concentrated under reduced pressure. The resulting mixture was concentrated to give the crude product, which was purified by silica gel column chromatography (eluting with 0–5% EtOAc in petroleum ether) to afford the product as a white solid (815 mg, 84%). ^{1}H NMR (400 MHz, Methanol-d_4) δ 8.27 (s, 1H), 8.21 (d, J = 8.4 Hz, 1H), 8.06 (d, J = 1.8 Hz, 1H), 7.91 (d, J = 7.4 Hz, 1H), 7.75 (t, J = 8.0 Hz, 1H), 7.59 (dd, J = 8.3, 1.8 Hz, 1H), 7.30 (d, J = 8.4 Hz, 1H), 2.40 (s, 3H). MS m/z: 358.12 ([M+H]$^+$).

*5.1.6. Compounds **19b-16g** was prepared with a similar procedure as that used for **19a***

*5.1.6.1. General procedure for the preparation of compounds **9a-g***

*5.1.6.1.1. N-(3-(1H-indazol-6-yl)-4-methylphenyl)-3-(trifluoromethyl) benzamide (**9a**).* To a resealable vial was added 6-(4,4,5,5-tetramethyl-1,3,2-dioxaborolan-2-yl)-1H-indazole (80 mg, 0.33 mmol), K_2CO_3(91 mg, 0.66 mmol), 19a (129 mg, 0.36 mmol). The vial was sealed and evacuated and purged with Ar for 5 min before addition of $PdCl_2$(dppf)-CH_2Cl_2 Adduct (15 mg, 0.02 mmol), dissolved in 1,4-dioxane/water (10 mL, 4:1, v/v) was then added to this solution before the vial was heated to 80 °C overnight. The reaction was cooled to room temperature, which was then brought to basic using aqueous sodium bicarbonate solution and extracted with ethyl acetate. The resulting mixture was concentrated to give the crude product, which was purified by silica gel column chromatography. Pale yellow solid. Yield: 64%. 1H NMR (400 MHz, Methanol-d4) δ 8.31 (s, 1H), 8.25 (d, J = 7.9 Hz, 1H), 8.08 (s, 1H), 7.92 (dt, J = 5.1, 2.3 Hz, 2H), 7.85 (d, J = 8.5 Hz, 1H), 7.80–7.72 (m, 2H), 7.58 (s, 1H), 7.47 (dd, J = 8.5, 1.3 Hz, 1H), 7.36 (s, 1H), 2.47 (s, 3H). ^{13}C NMR (126 MHz, DMSO-d_6) δ 164.31, 142.22, 140.45, 139.54, 137.11, 136.23, 133.89, 132.26, 131.02, 130.98, 130.19, 129.64 (d, J = 32.0 Hz), 128.56 (d, J = 4.0 Hz), 124.63 (d, J = 4.2 Hz), 124.45 (d, J = 272.5 Hz), 122.48, 122.33, 122.27, 120.66, 119.88, 110.24, 20.16.MS m/z: 396.2 ([M+H] $^+$), HRMS m/z (ESI) found 396.1313(M + H)$^+$, $C_{22}H_{17}F_3N_3O^+$ calcd for 396.1318, retention time 3.58 min, 100% pure.

*5.1.7. Compounds **9b-9g** was prepared with a similar procedure as that used for **9a***

*5.1.7.1. N-(3-(1H-indazol-6-yl)-5-methylphenyl)-3-(trifluoromethyl) benzamide (**9b**).* White solid, Yield: 70%. ^{1}H NMR (400 MHz, Methanol-d4) δ 8.31 (s, 1H), 8.25 (d, J = 7.9 Hz, 1H), 8.08 (s, 1H), 7.92–7.90 (m, 2H), 7.85 (d, J = 8.5 Hz, 1H), 7.80–7.72 (m, 2H), 7.58 (s, 1H), 7.47 (dd, J = 8.5, 1.3 Hz, 1H), 7.36 (s, 1H), 2.47 (s, 3H). ^{13}C NMR (151 MHz, Methanol-d4) δ 167.65, 143.87, 142.70, 141.81, 140.91, 140.53, 137.84, 135.29, 132.82, 132.51 (d, J = 32.7 Hz), 131.14, 129.82, 126.19, 126.07 (d, J = 3.9 Hz), 125.87 (d, J = 271.2 Hz), 124.19, 122.56, 122.40, 119.14, 109.50, 22.19.HRMS m/z (ESI) found 396.1324(M + H)$^+$, $C_{22}H_{17}F_3N_3O^+$ calcd for 396.1318, retention time 3.77 min, >98% pure.

*5.1.7.2. N-(5-(1H-indazol-6-yl)-2-methylphenyl)-3-(trifluoromethyl) benzamide (**9c**).* White solid, Yield: 77%. ^{1}H NMR (400 MHz, Methanol-d_4) δ 8.35 (s, 1H), 8.30 (d, J = 7.9 Hz, 1H), 8.07 (s, 1H), 7.95 (d, J = 7.6 Hz, 1H), 7.85 (d, J = 8.5 Hz, 1H), 7.82–7.75 (m, 2H), 7.73 (s, 1H), 7.60 (dd, J = 8.1, 1.9 Hz, 1H), 7.48 (d, J = 8.7 Hz, 1H), 7.44 (d, J = 7.9 Hz, 1H), 2.39 (s, 3H). ^{13}C NMR (126 MHz, Methanol-d4) δ 166.13, 140.85, 139.75, 139.32, 135.88, 135.31, 133.46, 133.39, 130.98, 130.91, 130.71 (d, J = 32.7 Hz), 129.35, 128.09 (d, J = 4.0 Hz), 125.61, 125.35, 124.24 (d, J = 4.2 Hz), 123.96 (d, J = 271.5 Hz), 122.22, 120.73, 120.47, 107.38, 16.49. HRMS m/z (ESI) found 396.133 (M + H)$^+$, $C_{22}H_{17}F_3N_3O^+$ calcd for 396.1318, retention time 3.62 min, >98% pure.

*5.1.7.3. N-(3-(1H-indazol-6-yl)-2-methylphenyl)-3-(trifluoromethyl) benzamide (**9d**).* Grey solid, Yield: 72%. ^{1}H NMR (400 MHz, Methanol-d4) δ 8.34 (s, 1H), 8.29 (d, J = 8.1 Hz, 1H), 8.11 (s, 1H), 7.94 (d, J = 7.6 Hz, 1H), 7.84 (dd, J = 8.3, 0.7 Hz, 1H), 7.77 (t, J = 7.9 Hz, 1H), 7.49 (s, 1H), 7.39 (t, J = 7.8 Hz, 1H), 7.34 (d, J = 7.7 Hz, 1H), 7.29 (dd, J = 7.4, 1.5 Hz, 1H), 7.17 (dd, J = 8.3, 1.2 Hz, 1H), 2.21 (s, 3H). ^{13}C NMR (151 MHz, Methanol-d4) δ 168.03, 145.50, 142.44, 142.16, 137.84, 137.16, 135.36, 134.30, 132.87, 132.59 (d, J = 32.4 Hz), 131.24, 130.36, 129.99, 127.80, 127.52, 126.11 (d, J = 4.3 Hz), 125.85 (d, J = 271.6 Hz), 124.55, 123.82, 121.92, 111.79, 16.62. HRMS m/z (ESI) found 396.1322 (M + H)$^+$, $C_{22}H_{17}F_3N_3O^+$ calcd for 396.1318. retention time 3.56min, >99% pure.

*5.1.7.4. N-(4-fluoro-3-(1H-indazol-6-yl) phenyl)-3-(trifluoromethyl) benzamide (**9e**).* White solid, Yield: 69%. ^{1}H NMR (400 MHz, Methanol-d4) δ 8.31 (s, 1H), 8.25 (d, J = 7.9 Hz, 1H), 8.11 (s, 1H), 7.98 (dd, J = 6.9, 2.6 Hz, 1H), 7.93 (d, J = 7.9 Hz, 1H), 7.88 (d, J = 8.5 Hz, 1H), 7.81–7.71 (m, 3H), 7.40 (d, J = 8.5 Hz, 1H), 7.31–7.22 (m, 1H). ^{13}C NMR (126 MHz, DMSO-d_6) δ 164.47, 155.93 (d, J = 243.4 Hz), 140.50, 136.04, 135.93, 133.95, 133.17, 132.30, 130.27, 129.69 (d, J = 32.2 Hz), 128.97 (d, J = 14.2 Hz), 128.73, 124.67 (d, J = 4.2 Hz), 124.44 (d, J = 272.4 Hz), 123.40, 122.78, 121.88, 121.81, 121.22, 116.80 (d,

J = 23.9 Hz), 110.49 (d, J = 3.2 Hz). HRMS m/z (ESI) found 400.1076 (M + H)$^+$, $C_{21}H_{14}F_4N_3O^+$ calcd for 400.1068, retention time 3.72min, >97% pure.

*5.1.7.5. N-(4-chloro-3-(1H-indazol-6-yl) phenyl)-3-(trifluoromethyl) benzamide (**9f**).* Yellow solid, Yield: 50%. ^{1}H NMR (400 MHz, Methanol-d_4) δ 8.29 (s, 1H), 8.23 (d, J = 8.0 Hz, 1H), 8.12 (s, 1H), 7.92 (d, J = 8.1 Hz, 1H), 7.89 (d, J = 2.7 Hz, 1H), 7.86 (d, J = 8.4 Hz, 1H), 7.82–7.76 (m, 1H), 7.72–7.77 (m, 1H), 7.63 (s, 1H), 7.55 (d, J = 8.7 Hz, 1H), 7.27 (d, J = 8.4 Hz, 1H). ^{13}C NMR (126 MHz, DMSO-d_6) δ 164.64, 140.73, 140.17, 138.46, 136.91, 135.93, 133.95, 132.35, 130.56, 130.28, 129.69 (d, J = 32.0 Hz), 128.81, 126.51, 124.70 (d, J = 4.1 Hz), 124.41 (d, J = 272.4 Hz), 123.80, 122.66, 122.42, 121.30, 120.78, 110.87. HRMS m/z (ESI) found 416.077 (M + H)$^+$, $C_{21}H_{14}ClF_3N_3O^+$ calcd for 416.0772, retention time 3.86min, >98% pure.

*5.1.7.6. N-(3-(1H-indazol-6-yl)-4-methoxyphenyl)-3-(trifluoromethyl) benzamide (**9g**).* Pale yellow solid, Yield: 50%. ^{1}H NMR (400 MHz, Methanol-d_4) δ 8.29 (s, 1H), 8.24 (d, J = 7.8 Hz, 1H), 8.07 (s, 1H), 7.91 (d, J = 8.0 Hz, 1H), 7.80 (d, J = 8.5 Hz, 1H), 7.78–7.74 (m, 2H), 7.74–7.68 (m, 2H), 7.35 (d, J = 9.0 Hz 1H), 7.15 (d, J = 8.8 Hz, 1H), 3.85 (s, 3H). ^{13}C NMR (126 MHz, Methanol-d4) δ 165.55, 153.91, 140.35, 137.08, 135.88, 133.31, 131.37, 130.97, 130.84, 130.60 (d, J = 32.8 Hz), 129.22, 127.83 (d, J = 4.3 Hz), 124.23, 124.09 (d, J = 3.8 Hz), 123.97 (d, J = 271.7 Hz), 122.97, 121.86, 121.77, 119.51, 111.63, 110.20, 55.02.HRMS m/z (ESI) found 412.1255 (M + H)$^+$, $C_{22}H_{17}ClF_3N_3O_2^+$ calcd for 412.1267, retention time 3.58 min, >97% pure.

*5.1.8. General procedure for the preparation of compounds **21a-g***

*5.1.8.1. 4-Methyl-3-(4,4,5,5-tetramethyl-1,3,2-dioxaborolan-2-yl)-N-(3-(trifluoromethyl)phenyl)benzamide (**21a**).*

4-methyl-3-(4,4,5,5-tetramethyl-1,3,2-dioxaborolan-2-yl) benzoic acid (8.95 g, 31 mmol) was stirred in a solvent of dimethyl formamide (25 mL).The reaction solution was added with HATU (12.98 g, 34.1 mmol), DIPEA (10.26 mL, 62.0 mmol) and 3-(trifluoromethyl)aniline (5 g, 31 mmol), followed by stirring for about 8 h at room temperature. The reaction mixture was diluted with ethyl acetate and washed with a saturated aqueous sodium bicarbonate solution and saline. The organic layer thus obtained was dried over anhydrous sodium sulfate, filtered, and concentrated under reduced pressure. The resulting mixture was concentrated to give the crude product, which was purified by silica gel column chromatography. White solid, Yield: 87%. ^{1}H NMR (400 MHz, DMSO-d_6) δ 10.55 (s, 1H), 8.24 (d, J = 2.0 Hz, 1H), 8.22 (d, J = 2.1 Hz, 1H), 8.10–8.03 (m, 1H), 7.97 (dd, J = 8.0, 2.2 Hz, 1H), 7.60 (t, J = 8.0 Hz, 1H), 7.45 (d, J = 7.7 Hz, 1H), 7.37 (d, J = 8.0 Hz, 1H), 2.55 (s, 3H), 1.33 (s, 12H). LC–MS m/z (ESI) found 406.3(M + H)$^+$

*5.1.9. Compounds **21b-21g** was prepared with a similar procedure as that used for **21a***

5.1.9.1. General procedure for the preparation of compounds 10a-i

*5.1.9.1.1. 3-(1H-indazol-6-yl)-4-methyl-N-(3-(trifluoromethyl) phenyl) benzamide (**10a**).* To a resealable vial was added K_2CO_3 (112.23 mg, 0.812 mmol), 6-bromo-1H-indazole (80 mg,0.406 mmol), S9a-h (1eq, 0.447 mmol). The vial was sealed and evacuated and purged with Ar (3X) before addition of $PdCl_2$(dppf)-CH_2Cl_2 Adduct (9.95 mg, 0.010 mmol), dissolved in dioxane (4 mL). Water (1 mL) was then added to this solution before the vial was heated to 80 °C overnight. The reaction was cooled to room temperature, diluted with EtOAc, filtered, and concentrated. The crude residue was purified via by silica gel column chromatography (eluting with 0–30% EtOAc in petroleum ether to afford the product as light grey solid. (10.3g, 82%). ^{1}H NMR (400 MHz, Methanol-d_4) δ 8.19 (s, 1H), 8.13 (s, 1H), 7.95 (d, J = 8.2 Hz, 1H), 7.92 (m, 2H), 7.88 (d, J = 8.3 Hz, 1H), 7.57 (d, J = 7.9 Hz, 1H), 7.54 (s, 1H), 7.50 (d, J = 8.5 Hz, 1H), 7.44 (d, J = 8.7 Hz, 1H), 7.20 (d, J = 9.0 Hz, 1H), 2.38 (s, 3H). ^{13}C NMR (151 MHz, Methanol-d4) δ 168.73, 143.78, 141.51, 141.20, 140.93, 134.92, 133.35, 132.09 (d, J = 32.0 Hz), 131.77, 130.65, 130.19, 127.77, 125.58 (d, J = 271.5 Hz), 125.20, 123.83, 123.48, 121.66, 118.47 (d, J = 4.1 Hz), 111.35, 20.80. HRMS m/z (ESI) found 396.1313 (M + H) $^+$, $C_{22}H_{17}F_3N_3O^+$ calcd for 396.1318; retention time 3.89 min, 100% pure.

*5.1.10. Compounds **10b-10i** was prepared with a similar procedure as that used for **10a***

*5.1.10.1. 3-(1H-indazol-6-yl)-N-(3-isopropylphenyl)-4-methyl benzamide (**10b**).* Pale yellow solid, Yield: 68%.^{1}H NMR (400 MHz, Methanol-d_4) δ 8.12 (s, 1H), 7.93–7.85 (m, 3H), 7.60 (s, 1H), 7.51–7.55 (m, 2H), 7.48 (d, J = 8.6 Hz, 1H), 7.28 (t, J = 7.9 Hz, 1H), 7.20 (d, J = 9.6 Hz, 1H), 7.05 (d, J = 7.7 Hz, 1H), 2.92 (p, J = 6.9 Hz, 1H), 2.37 (s, 3H), 1.29 (d, J = 6.9 Hz, 6H). ^{13}C NMR (126 MHz, DMSO-d_6) δ 164.93, 148.76, 141.55, 139.97, 139.14, 138.95, 138.50, 133.43, 132.42, 130.43, 128.77, 128.41, 126.70, 122.09, 121.90, 121.69, 120.24, 118.32, 117.99, 110.08, 33.49, 23.86, 20.28.HRMS m/z (ESI) found 370.1914 (M + H)$^+$, $C_{24}H_{24}N_3O^+$ calcd for 370.1914, retention time 3.96 min, 100% pure.

*5.1.10.2. N-(3-(2-cyanopropan-2-yl)phenyl)-3-(1H-indazol-6-yl)-4-methylbenzamide (**10c**).* Pale yellow solid, Yield: 74%.^{1}H NMR (400 MHz, Methanol-d_4) δ 8.10 (s, 1H), 7.97 (s, 1H), 7.92–7.87 (m, 2H), 7.84 (d, J = 8.3 Hz,1H), 7.71 (d, J = 8.1 Hz, 1H), 7.53 (s, 1H), 7.45 (d, J = 8.5 Hz, 1H), 7.39 (t, J = 8.0 Hz, 1H), 7.30 (d, J = 8.8 Hz, 1H), 7.16 (d, J = 8.3 Hz, 1H), 2.34 (s, 3H), 1.73 (s, 6H). ^{13}C NMR (151 MHz, Methanol-d4) δ 166.81, 141.91, 141.86, 139.80, 139.44, 139.37, 138.74, 133.02, 131.70, 129.86, 128.56, 128.25, 125.86, 123.74, 121.96, 121.58, 120.27, 119.76, 119.63, 117.13, 109.45, 36.57, 27.49, 18.90.HRMS m/z (ESI) found 395.1869 (M + H)$^+$, $C_{25}H_{23}N_4O^+$ calcd for 395.1866, retention time 3.81min, >99% pure.

*5.1.10.3. 3-(1H-indazol-6-yl)-4-methyl-N-(3-(trifluoromethyl) benzyl) benzamide (**10d**).* Grey Solid. Yield: 70%. ^{1}H NMR (400 MHz, Methanol-d_4) δ 8.10 (s, 1H), 7.88–7.76 (m, 3H), 7.68 (s, 1H), 7.63 (d, J = 7.0 Hz, 1H), 7.59–7.51 (m, 2H), 7.49 (s, 1H), 7.42 (d, J = 8.1 Hz, 1H), 7.14 (d, J = 8.3,1H), 4.65 (s, 2H), 2.33 (s, 3H). ^{13}C NMR (151 MHz, Methanol-d4) δ 168.11, 141.87, 139.96, 139.79, 139.39, 139.23, 133.00, 130.95, 130.44, 129.88 (d, J = 31.9 Hz), 129.83, 128.46, 127.97, 125.48, 123.80 (d, J = 271.3 Hz), 123.34 (d, J = 4.1 Hz), 123.01 (d, J = 4.0 Hz), 121.93, 121.55, 119.72, 109.39, 42.17, 18.84.HRMS m/z (ESI) found 410.147 (M + H)$^+$, $C_{23}H_{19}F_3N_3O^+$ calcd for 410.1475, retention time 3.99 min, >99% pure.

*5.1.10.4. 3-(1H-indazol-6-yl)-4-methyl-N-(3-(4-methylpiperazin-1-yl) phenyl) benzamide (**10e**).* Pale yellow solid, Yield: 74%.^{1}H NMR (400 MHz, Methanol-d4) δ 8.12 (s, 1H), 7.91–7.84 (m, 3H), 7.53 (s, 1H), 7.52–7.43 (m, 2H), 7.27 (t, J = 8.0 Hz, 1H), 7.20 (m, 2H), 6.83 (d, J = 8.7 Hz, 1H), 3.39 (t, J = 5.0 Hz, 4H), 3.12 (t, J = 5.0 Hz, 4H), 2.73 (s, 3H), 2.37 (s, 3H). ^{13}C NMR (126 MHz, DMSO-d_6) δ 164.88, 151.26, 141.55, 139.97, 139.89, 138.92, 138.49, 133.43, 132.47, 130.43, 128.89, 128.72, 126.68, 122.09, 121.90, 120.23, 111.10, 111.02, 110.08, 107.44, 54.53, 48.10, 45.68, 20.27.HRMS m/z (ESI) found 426.2289 (M + H)$^+$, $C_{26}H_{28}N_5O^+$ calcd for 426.2288, retention time 2.80min, >99% pure.

*5.1.10.5. 3-(1H-indazol-6-yl)-4-methyl-N-(4-(4-methylpiperazin-1-yl) phenyl) benzamide (**10f**).* Grey solid, Yield: 60%. ^{1}H NMR (400 MHz, Methanol-d4) δ 8.12 (s, 1H), 7.91–7.84 (m, 3H), 7.57 (d, J = 8.8 Hz, 2H), 7.52 (s, 1H), 7.47 (d, J = 8.5 Hz, 1H), 7.19 (d, J = 8.4 Hz, 1H), 7.00 (d, J = 9.0 Hz, 2H), 3.21 (t, J = 5.0 Hz, 4H), 2.66 (t, J = 5.0 Hz, 4H), 2.38 (s, 3H), 2.36 (s, 3H). ^{13}C NMR (151 MHz, Methanol-d4)

δ 166.51, 147.73, 147.08, 141.80, 139.81, 139.45, 139.09, 133.02, 131.94, 130.64, 129.79, 128.15, 125.70, 121.97, 121.74, 121.57, 119.73, 115.82, 109.42, 54.06, 48.37, 45.93, 18.87.HRMS *m/z* (ESI) found 426.2282 $(M + H)^+$, $C_{26}H_{28}N_5O^+$ calcd for 426.2288, retention time 2.70 min, >99% pure.

5.1.10.6. 3-(1H-indazol-6-yl)-4-methyl-N-(3-(4-methylpiperazin-1-yl) benzyl) benzamide ***(10g)***. Grey solid, Yield: 64%. ^{1}H NMR (400 MHz, Methanol-d4) δ 8.11 (s, 1H), 7.86 (d, $J = 8.4$ Hz 1H), 7.78–7.82 (m, 2H), 7.50 (s, 1H), 7.44 (d, $J = 9.2$ Hz, 1H), 7.24 (m, 1H), 7.17 (d, $J = 8.5$ Hz, 1H), 7.02 (s, 1H), 6.90 (d, $J = 9.4$ Hz, 2H), 4.55 (s, 2H), 3.26 (m, 4H), 2.81 (m, 4H), 2.50 (s, 3H), 2.35 (s, 3H). ^{13}C NMR (126 MHz, DMSO-d_6) δ 165.82, 150.81, 141.48, 140.42, 139.94, 138.55, 138.45, 133.39, 132.04, 130.36, 128.83, 128.51, 126.29, 122.06, 121.84, 120.19, 118.00, 114.52, 113.95, 110.01, 54.23, 47.75, 45.44, 42.92, 20.20.HRMS *m/z* (ESI) found 440.2442 $(M + H)^+$, $C_{27}H_{30}N_5O^+$ calcd for 440.2445, r etention time 2.53 min, >98% pure.

5.1.10.7. 3-(1H-indazol-6-yl)-4-methyl-N-(4-((4-methylpiperazin-1-yl) methyl) phenyl) benzamide ***(10h)***. Pale yellow solid, Yield: 70%. ^{1}H NMR (400 MHz, Methanol-d_4) δ 8.12 (s, 1H), 7.91–7.83 (m, 3H), 7.68 (d, $J = 8.4$ Hz, 2H), 7.52 (s, 1H), 7.47 (d, $J = 8.5$ Hz, 1H), 7.34 (s, 1H), 7.32 (s, 1H), 7.18 (d, $J = 8.9$ Hz, 1H), 3.54 (s, 2H), 2.57 (brs, 8H), 2.36 (s, 3H), 2.35 (s, 3H). ^{13}C NMR (151 MHz, Methanol-*d*4) δ 166.68, 141.81, 139.82, 139.36, 139.30, 137.42, 133.02, 132.27, 131.82, 129.84, 129.16, 128.25, 125.81, 121.97, 121.57, 120.32, 119.76, 109.47, 61.12, 53.51, 50.97, 43.53, 18.92.HRMS *m/z* (ESI) found 440.2441 $(M + H)^+$, $C_{27}H_{30}N_5O^+$ calcd for 440.2445, retention time 2.70 min, >99% pure.

5.1.10.8. 3-(1H-indazol-6-yl)-4-methyl-N-(3-((4-methylpiperazin-1-yl) methyl) phenyl) benzamide ***(10i)***. Pale yellow solid, Yield: 67%. ^{1}H NMR (400 MHz, Methanol-d_4) δ 8.13 (s, 1H), 7.90 (m, 2H), 7.87 (s, 1H), 7.80 (s, 1H), 7.58 (d, $J = 9.4$ Hz, 1H), 7.54 (s, 1H), 7.49 (d, $J = 8.6$ Hz, 1H), 7.35 (t, $J = 7.8$ Hz, 1H), 7.20 (d, $J = 8.1$ Hz, 1H), 7.16 (d, $J = 7.6$ Hz, 1H), 3.66 (s, 2H), 3.04 (brs, 4H), 2.69 (m, 7H), 2.38 (s, 3H). ^{13}C NMR (126 MHz, Methanol-*d*4) δ 168.69, 143.80, 141.74, 141.30, 140.12, 138.70, 134.99, 134.95, 133.71, 131.75, 130.12, 129.93, 127.68, 126.55, 123.84, 123.50, 123.34, 121.67, 121.66, 111.34, 62.93, 55.14, 51.81, 44.38, 20.76.HRMS *m/z* (ESI) found 440.2448 $(M + H)^+$, $C_{27}H_{30}N_5O^+$ calcd for 440.2445, retention time 2.78 min, >99% pure.

*5.1.10.9. 3-Bromo-N-(3-(hydroxymethyl)-5-(trifluoromethyl) phenyl)-4-methylbenzamide (****23****).* 3-bromo-4-methylbenzoic acid (9 g, 41.85 mmol) was stirred in a solvent of dimethyl formamide (35 mL). The reaction solution was added with HATU (17.5 g,46.04 mmol), DIPEA (15 mL, 83.70 mmol) and stirred for about 20 min at room temperature. The reaction solution was then added dropwise to a stirred solution of (3-amino-5-(trifluoromethyl) phenyl) methanol (8g, 41.85 mmol, **22**) at 0 °C, over a period of 30 min under nitrogen. The resulting solution was stirred at ambient temperature for 6 h. The reaction mixture was diluted with ethyl acetate and washed with a saturated aqueous sodium bicarbonate solution and saline. The organic layer thus obtained was dried over anhydrous sodium sulfate, filtered, and concentrated under reduced pressure. The resulting mixture was concentrated to give the crude product, which was purified by silica gel column chromatography (eluting with 0–30% EtOAc in petroleum ether) to provide **23** as a white solid (12g, 80%). ^{1}H NMR (400 MHz, DMSO-d_6) δ 10.55 (s, 1H), 8.24 (s, 1H), 8.12 (s, 1H), 8.04 (s, 1H), 7.92 (d, $J = 9.4$ Hz, 1H), 7.54 (d, $J = 7.9$ Hz, 1H), 7.40 (s, 1H), 4.60 (d, $J = 5.6$ Hz, 2H), 2.43 (s, 3H). MS *m/z*: 388.1([M+H] $^+$).

*5.1.10.10. 3-Bromo-N-(3-(bromomethyl)-5-(trifluoromethyl) phenyl)-4-methylbenzamide (****24****).* A mixture of **23** (10 g, 25.76 mmol) and triphenylphosphine (8.11 g,30.91 mmol) was stirred in dry acetonitrile (30 mL) for 15 min. NBS (5.50 g, 30.91 mmol) was added and the stirring continued at ambient temperature for 4 h. The reaction was quenched by addition of H_2O and then extracted with ethyl acetate. The combined organic layer was washed with brine, dried over Na_2SO_4 and concentrated. The crude product was purified by column chromatography on silica gel with petroleum ether or mixture of petroleum ether and ethyl acetate (30%) as eluent to afford the white solids. (10g, 86%). ^{1}H NMR (400 MHz, Chloroform-d) δ 8.06 (d, $J = 1.9$ Hz, 1H), 7.99 (q, $J = 3.1$, 2.5 Hz, 2H), 7.86 (s, 1H), 7.73 (dd, $J = 7.9$, 1.9 Hz, 1H), 7.45 (s, 1H), 7.38 (d, $J = 8.0$ Hz, 1H), 4.52 (s, 2H), 2.50 (s, 3H). LRMS *m/z*: 450/452/454 ([M+H] $^+$).

5.1.11. General procedure for the preparation of compounds ***25j-m***

*5.1.11.1. 3-Bromo-4-methyl-N-(3-((4-methylpiperazin-1-yl)methyl)-5-(trifluoromethyl)phenyl)benzamide(****25j****).* A mixture of 24 (1 g, 2.22 mmol) and triethylamine (616 μl, 4.43 mmol) was stirred in dry dichloromethane. 1-methylpiperazine (289 mg, 2.88 mmol) was added and the stirring continued at ambient temperature for 2 h. The reaction was quenched by addition of H_2O and then extracted with dichloromethane. The combined organic layer was washed with brine, dried over Na_2SO_4 and concentrated. The resulting mixture was concentrated and purified by silica gel column chromatography (eluting with 0–3% MeOH in DCM).Yellow oil, Yield: 70%. ^{1}H NMR (400 MHz, Methanol-d_4) δ 8.14 (d, $J = 1.7$ Hz, 1H), 8.08 (s, 1H), 7.92 (s, 1H), 7.84 (dd, $J = 7.9$, 1.8 Hz, 1H), 7.47–7.36 (m, 2H), 3.61 (s, 2H), 2.79–2.46 (brs, 8H), 2.45 (s, 3H), 2.37 (s, 3H). LRMS *m/z*: 470.4 ([M+H] $^+$).

5.1.12. Compounds ***25k-10m*** *was prepared with a similar procedure as that used for* ***25j***

5.1.12.1. General procedure for the preparation of compounds ***10j-m***

*5.1.12.1.1. 3-(1H-indazol-6-yl)-4-methyl-N-(3-((4-methylpiperazin-1-yl)methyl)-5-(trifluoromethyl)phenyl)benzamide (****10j****).* To a resealable vial was added 6-(4,4,5,5-tetramethyl-1,3,2-dioxaborolan-2-yl)-1H-indazole (78 mg, 0.319 mmol), K_2CO_3(88 mg, 0.638 mmol), 25j (150 mg, 0.319 mmol). The vial was sealed and evacuated and purged with Ar for 5min before addition of $PdCl_2$(dppf)-CH_2Cl_2 Adduct (15 mg, 0.015 mmol), dissolved in 1,4-dioxane/water (10 mL, 4:1, v/v) was then added to this solution before the vial was heated to 80 °C overnight. The reaction was cooled to room temperature, which was then brought to basic using aqueous sodium bicarbonate solution and extracted with ethyl acetate. The resulting mixture was concentrated to give the crude product, which was purified by silica gel column chromatography. Brown solid (123 mg, 76%).^{1}H NMR (400 MHz, Methanol-d_4) δ 8.12 (s, 1H), 8.10 (s, 1H), 7.95 (s, 1H), 7.93–7.90 (m, 2H), 7.88 (d, $J = 8.3$ Hz, 1H), 7.54 (s, 1H), 7.50 (d, $J = 8.4$ Hz, 1H), 7.44 (s, 1H), 7.20 (d, $J = 8.2$ Hz, 1H), 3.64 (s, 2H), 2.60 (brs, 8H), 2.38 (s, 3H), 2.36 (s, 3H). ^{13}C NMR (126 MHz, DMSO-d_6) δ 165.86, 142.13, 141.05, 140.49, 140.44, 139.95, 138.86, 133.92, 132.26, 131.03, 129.65 (d, $J = 33.2$ Hz), 129.33, 129.29, 127.32, 124.66 (d, $J = 272.3$ Hz), 122.54, 122.40, 120.75, 120.39, 115.61, 110.58, 61.81, 54.93, 52.69, 45.86, 20.79.HRMS *m/z* (ESI) found 508.231 $(M + H)^+$, $C_{28}H_{29}F_3N_5O^+$ calcd for 508.2319; retention time 2.88 min, 100% pure.

*5.1.12.1.2. N-(3-((4-ethylpiperazin-1-yl)methyl)-5-(trifluoromethyl)phenyl)-3-(1H-indazol-6-yl)-4-methylbenzamide (****10k****).* Yellow solid, Yield: 78%. ^{1}H NMR (400 MHz, Methanol-d_4) δ 8.13 (s, 1H), 8.11 (s, 1H), 7.94 (s, 1H), 7.93–7.90 (m, 2H), 7.87 (d, $J = 8.5$ Hz,1H), 7.54 (s, 1H), 7.50 (d, $J = 8.5$ Hz, 1H), 7.44 (s, 1H), 7.20 (d, $J = 8.3$ Hz, 1H), 3.64 (s, 2H), 2.74–2.46 (m, 10H), 2.38 (s, 3H), 1.13 (t, $J = 7.2$ Hz, 3H). ^{13}C NMR (151 MHz, Methanol-*d*4) δ 166.82, 141.92, 139.80, 139.66, 139.31, 139.23, 139.09, 133.03, 131.45, 130.25

(d, $J = 32.0$ Hz), 129.90, 128.29, 125.88, 124.05, 123.66 (d, $J = 271.4$ Hz), 121.93, 121.60, 120.48, 119.78, 115.56, 109.43, 61.16, 51.56, 51.45, 51.35, 18.90, 9.70.HRMS *m/z* (ESI) found 522.2475 (M + H) $^+$, $C_{29}H_{31}F_3N_5O^+$ calcd for 522.2475, retention time 2.91 min, >99% pure.

*5.1.12.1.3. N-(3-((4-(2-hydroxyethyl)piperazin-1-yl)methyl)-5-(trifluoromethyl)phenyl)-3-(1H-indazol-6-yl)-4-methyl benzamide (**10l**).* Yellow solid, Yield: 50%.^{1}H NMR (400 MHz, Methanol-d_4) δ 8.13 (s, 1H), 8.09 (s, 1H), 7.97 (s, 1H), 7.93–7.89 (m, 2H), 7.87 (d, $J = 8.3$ Hz, 1H),7.54 (s, 1H), 7.50 (d, $J = 8.0$ Hz, 1H), 7.45 (s, 1H), 7.20 (d, $J = 8.4$ Hz, 1H), 3.71 (t, $J = 5.9$ Hz, 2H), 3.62 (s, 2H), 2.78–2.45 (m, 10H), 2.37 (s, 3H). ^{13}C NMR (151 MHz, Methanol-*d*4) δ 166.81, 141.91, 139.81, 139.66, 139.30, 139.16, 139.09, 133.02, 131.44, 130.25 (d, $J = 32.2$ Hz), 129.90, 128.29, 125.88, 124.06, 123.65 (d, $J = 268.7$ Hz), 121.93, 121.59, 120.49, 119.79, 115.58, 109.46, 61.12, 59.09, 57.38, 52.28, 51.29, 18.91.HRMS *m/z* (ESI) found 538.2418 (M + H) $^+$, $C_{29}H_{31}F_3N_5O_2^+$ calcd for 538.2424, retention time 2.83 min, >98% pure.

5.1.12.1.4. N-(3-((4-cyclopentylpiperazin-1-yl)methyl)-5-(trifluoromethyl)phenyl)-3-(1H-indazol-6-yl)-4-methylbenzamide(10 m). Pale yellow solid, Yield: 56%. ^{1}H NMR (400 MHz, Methanol-d_4) δ 8.12 (s, 1H), 8.10 (s, 1H), 7.94 (s, 1H), 7.91 (m, 2H), 7.87 (d, $J = 8.5$ Hz, 1H), 7.53 (s, 1H), 7.49 (d, $J = 8.5$ Hz, 1H), 7.43 (s, 1H), 7.19 (d, $J = 8.5$ Hz, 1H), 3.62 (s, 2H), 2.79–2.41 (m, 9H), 2.37 (s, 3H), 1.91 (m, 2H), 1.72 (m, 2H), 1.60 (m, 2H), 1.41 (m, 2H). ^{13}C NMR (151 MHz, Methanol-*d*4) δ 166.82, 141.93, 139.80, 139.66, 139.31, 139.16, 139.09, 133.03, 131.46, 130.46 (d, $J = 31.5$ Hz), 129.90, 128.29, 125.89, 124.08, 121.93, 120.52, 119.79, 115.56, 109.43, 67.00, 61.18, 51.47, 51.22, 29.07, 23.13, 18.90.HRMS *m/z* (ESI) found 562.2787 (M + H) $^+$, $C_{32}H_{35}F_3N_5O^+$ calcd for 562.2788, retention time 3.03 min, >98% pure.

*5.1.13. General procedure for the preparation of compounds **27a-r***

*5.1.13.1. 6-Bromo-3-(1-cyclopropyl-1H-pyrazol-4-yl)-1H-indazole (**27k**).* To a resealable vial was added K_2CO_3 (1.71 g, 12.4 mmol), 6-bromo-3-iodo-1H-indazole (2 g, 6.2 mmol), 41-cyclopropyl-4-(4,4,5,5-tetramethyl-1,3,2-dioxaborolan-2-yl)-1H-pyrazole(1.45 g, 6.2 mmol). The vial was sealed and evacuated and purged with Ar for 5 min before addition of $PdCl_2$(dppf)-CH_2Cl_2 Adduct (253 mg, 0.310 mmol), dissolved in 1,4-dioxane/water (10 mL, 4:1, v/v) was then added to this solution before the vial was heated to 80 °C overnight. The reaction was cooled to room temperature, which was then brought to basic using aqueous sodium bicarbonate solution and extracted with ethyl acetate. The resulting mixture was concentrated to give the crude product, which was purified by silica gel column chromatography. The resulting mixture was concentrated to give the crude product, which was purified by silica gel column chromatography. Pale yellow solid(1.2 g, 64%). ^{1}H NMR (400 MHz, Chloroform-d) δ 8.04 (s, 1H), 7.99 (s, 1H), 7.70 (d, $J = 8.6$ Hz, 1H), 7.52 (d, $J = 1.5$ Hz, 1H), 7.27 (dd, $J = 8.8$, 1.4 Hz, 1H), 3.71 (tt, $J = 7.4$, 3.8 Hz, 1H), 1.25–1.18 (m, 2H), 1.13–1.03 (m, 2H). LRMS *m/z*: 303 ([M+H] $^+$).

*5.1.14. Compounds **25a-27r** was prepared with a similar procedure as that used for **27k***

*5.1.14.1. General procedure for the preparation of compounds **11a-r***

*5.1.14.1.1. 4-Methyl-3-(3-(4-(4-methylpiperazin-1-yl)phenyl)-1H-indazol-6-yl)-N-(3-(trifluoromethyl)phenyl)benzamide (**11a**).* To a resealable vial was added **27a** (120 mg, 0.32 mmol), K_2CO_3 (90 mg, 0.65 mmol) and **21a** (131 mg, 0.32 mmol). The vial was sealed and evacuated and purged with Ar for 5 min before addition of $PdCl_2$(dppf)-CH_2Cl_2 Adduct (15 mg, 0.02 mmol), dissolved in 1,4-dioxane/water (10 mL, 4:1, v/v) was then added to this solution before the vial was heated to 80 °C overnight. The reaction was cooled to room temperature, which was then brought to basic using aqueous sodium bicarbonate solution and extracted with ethyl acetate. The resulting mixture was concentrated to give the crude product, which was purified by silica gel column chromatography. The crude residue was purified via by silica gel column chromatography (eluting with 0–10% MeOH in DCM) to afford the product as white solid (110 mg, 60%). ^{1}H NMR (400 MHz, Chloroform-*d*) δ 8.31 (s, 1H), 8.01 (d, $J = 8.4$ Hz, 1H), 7.97 (s, 1H), 7.91–7.86 (m, 3H), 7.83 (dd, $J = 7.9$, 1.9 Hz, 1H), 7.79 (d, $J = 1.8$ Hz, 1H), 7.45 (t, $J = 7.9$ Hz, 1H), 7.42–7.33 (m, 2H), 7.29 (s, 1H), 7.14 (dd, $J = 8.3$, 1.2 Hz, 1H), 7.03 (d, $J = 8.9$ Hz, 2H), 3.28 (t, $J = 5.0$ Hz, 4H), 2.64 (t, $J = 5.0$ Hz, 4H), 2.39 (s, 3H), 2.33 (s, 3H). ^{13}C NMR (126 MHz, DMSO-d_6) δ 165.91, 150.87, 143.90, 142.15, 142.00, 140.46, 139.98, 138.84, 132.34, 131.07, 130.30, 129.79 (d, $J = 31.6$ Hz), 129.33, 127.94, 127.35, 124.66, 124.63 (d, $J = 272.0$ Hz), 124.26, 122.87, 121.08, 120.35, 119.57, 116.90, 115.86, 110.92, 54.91, 48.12, 46.03, 20.81. ·HRMS *m/z* (ESI) found 570.2481 (M + H)$^+$, $C_{33}H_{31}F_3N_5O^+$ calcd for 570.2475, retention time 3.42 min, 100% pure.

*5.1.14.1.2. 4-Methyl-3-(3-(4-(4-methylpiperazine-1-carbonyl)phenyl)-1H-indazol-6-yl)-N-(3-(trifluoromethyl)phenyl)benzamide (**11b**).* Light brown Solid, Yield: 45%,^{1}H NMR (400 MHz, Methanol-*d*4) δ 8.20 (s, 1H), 8.12 (m, 3H), 7.95 (d, $J = 9.2$ Hz, 1H), 7.93 (d, $J = 1.8$ Hz, 1H), 7.91 (dd, $J = 7.9$, 1.9 Hz, 1H), 7.61 (s, 1H), 7.59 (s, 1H), 7.56 (s, 1H), 7.53 (d, $J = 8.0$ Hz, 1H), 7.48 (d, $J = 7.9$ Hz, 1H), 7.43 (d, $J = 7.8$ Hz, 1H), 7.26 (dd, $J = 8.4$, 1.3 Hz, 1H), 3.82 (brs, 2H), 3.57 (brs, 2H), 2.52 (d, $J = 36.0$ Hz, 4H), 2.38 (s, 3H), 2.35 (s, 3H). ^{13}C NMR (151 MHz, Methanol-*d*4) δ 170.31, 166.75, 143.00, 141.58, 141.56, 139.60, 139.36, 139.04, 134.94, 134.02, 131.52, 130.20 (d, $J = 32.3$ Hz), 129.94, 128.77, 128.31, 126.95, 126.60, 125.97, 123.68 (d, $J = 271.6$ Hz), 123.29, 122.73, 119.77, 119.03, 116.57, 109.94, 44.11, 18.95. HRMS *m/z* (ESI) found 598.2428 (M + H)$^+$, $C_{34}H_{31}F_3N_5O_2^+$ calcd for 598.2424, retention time 3.25 min, >99% pure.

*5.1.14.1.3. 4-Methyl-3-(3-(4-((4-methylpiperazin-1-yl)methyl)phenyl)-1H-indazol-6-yl)-N-(3-(trifluoromethyl)phenyl)benzamide (**11c**).* Yellow solid, Yield:50%. ^{1}H NMR (400 MHz, Methanol-d_4) δ 8.23 (s, 1H), 8.03 (d, $J = 8.2$ Hz, 1H), 7.95 (d, $J = 7.9$ Hz, 3H), 7.92–7.88 (m, 2H), 7.56 (s, 1H), 7.53 (t, $J = 7.9$ Hz, 1H), 7.50–7.46 (d, $J = 7.5$ Hz,2H), 7.42 (m, 2H), 7.19 (d, $J = 8.1$ Hz, 1H), 3.64 (s, 2H), 2.95 (brs, 4H), 2.70 (brs, 4H), 2.61 (s, 3H), 2.33 (s, 3H). ^{13}C NMR (151 MHz, Methanol-*d*4) ^{13}C NMR (151 MHz, Methanol-*d*4) δ 171.09, 166.74, 143.91, 141.66, 141.52, 139.60, 139.28, 139.05, 136.55, 132.08, 131.49, 130.19 (d, $J = 32.1$ Hz), 129.92, 129.29, 128.77, 128.32, 126.51, 125.93, 123.68 (d, $J = 271.6$ Hz), 123.28, 122.43, 119.97, 119.03, 116.54 (q, $J = 3.6$ Hz), 109.86, 61.63, 59.67, 53.78, 51.62, 18.98. .HRMS *m/z* (ESI) found 584.2633 (M + H)$^+$, $C_{34}H_{33}F_3N_5O^+$ calcd for 584.2632, retention time 3.16 min, >99% pure.

*5.1.14.1.4. 4-Methyl-3-(3-(4-morpholinophenyl)-1H-indazol-6-yl)-N-(3-(trifluoromethyl)phenyl)benzamide (**11d**).* White solid, Yield: 47%,^{1}H NMR (400 MHz, Chloroform-*d*) δ 8.31 (s, 1H), 8.04 (d, $J = 8.4$ Hz, 1H), 7.98 (s, 1H), 7.95–7.88 (m, 3H), 7.85–7.78 (m, 2H), 7.48 (t, $J = 8.0$ Hz, 1H), 7.42 (dd, $J = 12.2$, 7.8 Hz, 2H), 7.20 (s, 1H), 7.17 (dd, $J = 8.4$, 1.4 Hz, 1H), 7.03 (d, $J = 8.5$ Hz, 2H),3.90 (t, $J = 4.9$ Hz, 4H), 3.16 (t, $J = 4.9$ Hz, 4H), 2.34 (s, 3H). ^{13}C NMR (151 MHz, Methanol-*d*4) δ 166.82, 150.84, 141.79, 139.64, 139.27, 139.05, 131.50, 130.21 (d, $J = 32.2$ Hz), 129.91, 128.77, 128.29, 127.44, 125.91, 124.58, 124.27, 123.30, 122.09, 120.17, 119.78, 118.97, 116.56 (d, $J = 4.2$ Hz), 115.02, 109.74, 66.09, 48.42, 18.94.HRMS *m/z* (ESI) found 557.2166 (M + H)$^+$, $C_{32}H_{28}F_3N_4O_2^+$ calcd for 557.2159, retention time 3.95min, >99% pure.

*5.1.14.1.5. 4-Methyl-3-(3-(4-(4-morpholinopiperidin-1-yl)phenyl)-1H-indazol-6-yl)-N-(3-(trifluoromethyl)phenyl)benzamide (**11e**).* Pale brown solid, Yield: 60%. ^{1}H NMR (400 MHz, Chloroform-*d*) δ 8.50 (s, 1H), 8.01 (d, $J = 7.8$ Hz, 2H), 7.92 (d, $J = 8.4$ Hz, 1H), 7.90–7.84 (m, 3H), 7.83 (d, $J = 2.0$ Hz, 1H), 7.46 (t, $J = 7.9$ Hz, 1H), 7.39 (t, $J = 7.1$ Hz, 2H), 7.28 (s, 1H), 7.14 (d, $J = 8.3$ Hz, 1H), 7.02 (d, $J = 8.6$ Hz, 2H), 3.80–3.77 (m, 4H), 2.73 (t, $J = 12.1$ Hz, 2H), 2.64 (d,

J = 5.4 Hz, 4H), 2.41 (d, J = 12.4 Hz, 1H), 2.33 (s, 3H), 1.98 (d, J = 12.4 Hz, 2H), 1.75–1.69 (m, 1H), 1.68 (d, J = 3.9 Hz, 1H), 1.37 (t, J = 7.3 Hz, 1H), 1.28 (s, 1H). ^{13}C NMR (126 MHz, DMSO-d_6) δ 165.92, 143.93, 142.14, 142.00, 140.47, 139.97, 138.82, 132.34, 131.07, 130.30, 129.79 (d, J = 31.5 Hz), 129.34, 127.97, 127.35, 124.63 (d, J = 272.2 Hz), 124.26, 122.84, 121.08, 120.33, 119.56,116.88, 116.14, 110.92, 66.99, 61.62, 49.20, 46.09, 27.30, 20.81.HRMS m/z (ESI) found 640.2907 (M + H)$^+$, $C_{37}H_{37}F_3N_5O_2^+$ calcd for 640.2894, retention time 3.38 min, >99% pure.

*5.1.14.1.6. 3-(3-(1H-pyrazol-4-yl)-1H-indazol-6-yl)-4-methyl-N-(3-(trifluoromethyl) phenyl) benzamide (**11f**).* Yellow solid, Yield: 40%,^{1}H NMR (400 MHz, Methanol-d_4) δ 8.28 (brs, 2H), 8.19 (s, 1H), 8.05 (d, J = 8.3 Hz, 1H), 7.97–7.87 (m, 3H), 7.59–7.52 (m, 1H), 7.51 (s, 1H), 7.47 (d, J = 7.9 Hz, 1H), 7.42 (d, J = 7.9 Hz, 1H), 7.22 (d, J = 8.3 Hz, 1H), 2.37 (s, 3H). ^{13}C NMR (126 MHz, DMSO-d_6) δ 165.91, 142.10, 141.65, 140.46, 139.98, 139.01, 138.40, 137.25, 132.32, 131.06, 130.29, 129.79 (d, J = 31.7 Hz), 129.31, 127.34, 126.47, 124.63 (d, J = 272.2 Hz), 124.26, 122.49, 120.90, 120.31, 119.71, 116.87, 114.74, 110.73, 20.80.HRMS m/z (ESI) found 462.1537 (M + H)$^+$, $C_{25}H_{19}F_3N_5O^+$ calcd for 462.1536, retention time 3.58 min, >99% pure.

*5.1.14.1.7. 4-Methyl-3-(3-(1-methyl-1H-pyrazol-4-yl)-1H-indazol-6-yl)-N-(3-(trifluoromethyl)phenyl)benzamide (**11g**).* Pink powder, Yield: 73%. ^{1}H NMR (400 MHz, Methanol-d_4) δ 8.27 (s, 1H), 8.20 (s, 1H), 8.10 (s, 1H), 8.06 (dd, J = 8.4, 0.9 Hz, 1H), 7.96 (d, J = 8.6 Hz, 1H), 7.94–7.91 (m, 2H), 7.56 (t, J = 8.0 Hz, 1H), 7.53–7.47 (m, 2H), 7.44 (d, J = 7.8 Hz, 1H), 7.25 (dd, J = 8.4, 1.4 Hz, 1H), 4.04 (s, 3H), 2.39 (s, 3H). ^{13}C NMR (126 MHz, DMSO-d_6) δ 165.90, 142.06, 141.62, 140.46, 139.99, 139.05, 138.05, 136.91, 132.31, 131.06, 130.30, 129.78 (d, J = 31.4 Hz), 129.32, 128.89, 127.35, 124.63 (d, J = 272.1 Hz), 124.26, 122.55, 120.76, 120.35, 119.60, 116.89, 115.39, 110.77, 39.10, 20.80. HRMS m/z (ESI) found 476.1704 (M + H) $^+$, $C_{26}H_{21}F_3N_5O^+$ calcd for 476.1693; retention time 3.79 min,100% pure.

*5.1.14.1.8. 3-(3-(1-ethyl-1H-pyrazol-4-yl)-1H-indazol-6-yl)-4-methyl-N-(3-(trifluoromethyl)phenyl)benzamide (**11h**).* White solid, Yield: 69%.^{1}H NMR (400 MHz, Methanol-d_4) δ 8.31 (s, 1H), 8.20 (s, 1H), 8.11 (s, 1H), 8.08 (dd, J = 8.4, 0.9 Hz, 1H), 7.96 (d, J = 8.6 Hz, 1H), 7.94–7.85 (m, 2H), 7.56 (t, J = 8.0 Hz, 1H), 7.54–7.48 (m, 2H), 7.44 (d, J = 7.8 Hz, 1H), 7.26 (dd, J = 8.4, 1.3 Hz, 1H), 4.33 (q, J = 7.3 Hz, 2H), 2.40 (s, 3H), 1.57 (t, J = 7.3 Hz, 3H). ^{13}C NMR (126 MHz, DMSO-d_6) δ 165.90, 142.07, 141.63, 140.46, 139.99, 139.04, 138.15, 136.77, 132.32, 131.07, 130.30, 129.78 (d, J = 31.5 Hz), 129.31, 127.42, 127.35, 124.63 (d, J = 272.6 Hz), 124.26, 122.51, 120.82, 120.35, 119.60, 116.90, 115.20, 110.76, 46.85, 20.80, 16.01.HRMS m/z (ESI) found 490.1849 (M + H) $^+$, $C_{27}H_{23}F_3N_5O^+$ calcd for 490.1849, retention time 3.90 min, >99% pure.

*5.1.14.1.9. 4-Methyl-3-(3-(1-propyl-1H-pyrazol-4-yl)-1H-indazol-6-yl)-N-(3-(trifluoromethyl)phenyl)benzamide (**11i**).* Pink powder, Yield: 69%. ^{1}H NMR (400 MHz, Methanol-d_4) δ 8.30 (s, 1H), 8.20 (s, 1H), 8.12 (s, 1H), 8.07 (dd, J = 8.4, 0.8 Hz, 1H), 7.96 (d, J = 8.7 Hz, 1H), 7.94–7.91 (m, 2H), 7.56 (t, J = 8.1 Hz, 1H), 7.53–7.47 (m, 2H), 7.44 (d, J = 7.0 Hz, 1H), 7.25 (dd, J = 8.4, 1.4 Hz, 1H), 4.25 (t, J = 7.0 Hz, 2H), 2.39 (s, 3H), 1.98 (h, J = 7.3 Hz, 2H), 0.99 (t, J = 7.4 Hz, 3H). ^{13}C NMR (126 MHz, DMSO-d_6) δ 165.91, 142.07, 141.63, 140.46, 139.99, 139.04, 138.14, 136.84, 132.32, 131.06, 130.30, 129.79 (d, J = 31.7 Hz), 129.30, 128.10, 127.35, 124.26, 122.52, 120.82, 120.32, 119.60, 116.87, 115.07, 110.76, 53.45, 23.72, 20.80, 11.45.HRMS m/z (ESI) found 504.2009 (M + H) $^+$, $C_{28}H_{25}F_3N_5O^+$ calcd for 504.2006, retention time 4.04 min, >99% pure.

*5.1.14.1.10. 3-(3-(1-isopropyl-1H-pyrazol-4-yl)-1H-indazol-6-yl)-4-methyl-N-(3-(trifluoromethyl)phenyl)benzamide (**11j**).* White solid, Yield: 74%. ^{1}H NMR (400 MHz, Methanol-d_4) δ 8.31 (s, 1H), 8.20 (s, 1H), 8.12 (s, 1H), 8.08 (dd, J = 8.4, 0.7 Hz, 1H), 7.96 (d, J = 8.1 Hz, 1H), 7.94–7.91 (m, 2H), 7.56 (t, J = 8.0 Hz, 1H), 7.53–7.47 (m, 2H), 7.44 (d, J = 8.4 Hz, 1H), 7.25 (dd, J = 8.4, 1.4 Hz, 1H), 4.68 (hept, J = 6.7 Hz, 1H), 2.39 (s, 3H), 1.61 (d, J = 6.7 Hz, 6H). ^{13}C NMR (126 MHz, DMSO-d_6) δ 165.91, 142.08, 141.63, 140.47, 139.99, 139.03, 138.25, 136.44, 132.32, 131.06, 130.29, 129.79 (d, J = 31.5 Hz), 129.31, 127.35, 125.69, 124.26, 122.47, 120.91, 120.32, 119.60, 116.87, 115.00, 110.73, 53.65, 23.20, 20.80. HRMS m/z (ESI) found 504.2004(M + H) $^+$, $C_{28}H_{25}F_3N_5O^+$ calcd for 504.2006, retention time 4.03 min, >99% pure.

*5.1.14.1.11. 3-(3-(1-cyclopropyl-1H-pyrazol-4-yl)-1H-indazol-6-yl)-4-methyl-N-(3-(trifluoromethyl)phenyl)benzamide (**11k**).* White Solid, Yield: 70%. ^{1}H NMR (400 MHz, DMSO-d_6) δ 13.06 (s, 1H), 10.52 (s, 1H), 8.45 (s, 1H), 8.25 (s, 1H), 8.14 (d, J = 8.3 Hz, 1H), 8.08 (d, J = 8.5 Hz, 1H), 8.02 (s, 1H), 7.98 (s, 1H), 7.95 (dd, J = 8.0, 1.7 Hz, 1H), 7.60 (t, J = 8.0 Hz, 1H), 7.55–7.49 (m, 2H), 7.45 (d, J = 7.6 Hz, 1H), 7.20 (dd, J = 8.3, 1.0 Hz, 1H), 3.84 (tt, J = 7.5, 3.9 Hz, 1H), 2.35 (s, 3H), 1.21–1.09 (m, 2H), 1.09–0.94 (m, 2H). ^{13}C NMR (126 MHz, DMSO-d_6) δ 165.44, 141.60, 141.15, 140.00, 139.54, 138.60, 137.48, 136.50, 131.85, 130.61, 129.85, 129.32 (d, J = 31.5 Hz), 128.85, 127.35, 126.90, 124.17 (d, J = 272.4 Hz), 124.21, 122.07, 120.47, 119.86, 119.11, 116.39, 114.78, 110.27, 32.90, 20.35, 6.35. ^{19}F NMR (471 MHz, DMSO-d_6) δ −61.26. HRMS m/z (ESI) found 502.1859 (M + H) $^+$, $C_{28}H_{23}F_3N_5O^+$ calcd for 502.1849; retention time 3.96 min, 100% pure.

*5.1.14.1.12. 3-(3-(1-(2-hydroxyethyl)-1H-pyrazol-4-yl)-1H-indazol-6-yl)-4-methyl-N-(3-(trifluoromethyl)phenyl)benzamide (**11l**).* Grey solid, Yield: 60%.^{1}H NMR (400 MHz, Methanol-d_4) δ 8.33 (s, 1H), 8.20 (s, 1H), 8.14 (s, 1H), 8.08 (dd, J = 8.4, 0.7 Hz, 1H), 7.96 (d, J = 8.7 Hz, 1H), 7.94–7.91 (m, 2H), 7.56 (t, J = 8.0 Hz, 1H), 7.52–7.47 (m, 2H), 7.44 (d, J = 8.4 Hz, 1H), 7.25 (dd, J = 8.4, 1.3 Hz, 1H), 4.38 (t, J = 5.4 Hz, 2H), 4.00 (t, J = 5.3 Hz, 2H), 2.39 (s, 3H). ^{13}C NMR (126 MHz, DMSO-d_6) δ 165.90, 142.06, 141.63, 140.46, 139.99, 139.04, 138.14, 136.93, 132.31, 131.07, 130.30, 129.78 (d, J = 31.5 Hz), 129.31, 128.61, 127.36, 124.63 (d, J = 272.1 Hz), 124.26, 122.53, 120.78, 120.34, 119.60, 116.90, 115.09, 110.78, 60.54, 54.63, 20.81.HRMS m/z (ESI) found 506.1806 (M + H) $^+$, $C_{27}H_{23}F_3N_5O_2^+$ calcd for 506.1798, retention time 3.53 min, >99% pure.

*5.1.14.1.13. 3-(3-(1-(2-hydroxypropyl)-1H-pyrazol-4-yl)-1H-indazol-6-yl)-4-methyl-N-(3-(trifluoromethyl)phenyl)benzamide (**11m**).* Grey solid, Yield: 53%. ^{1}H NMR (400 MHz, Methanol-d_4) δ 8.31 (s, 1H), 8.20 (s, 1H), 8.13 (s, 1H), 8.08 (dd, J = 8.4, 0.9 Hz, 1H), 7.96 (d, J = 6.9 Hz, 1H), 7.94–7.90 (m, 2H), 7.56 (t, J = 8.0 Hz, 1H), 7.54–7.49 (m, 2H), 7.44 (d, J = 8.5 Hz, 1H), 7.26 (dd, J = 8.4, 1.4 Hz, 1H), 4.30–4.17 (m, 3H), 2.40 (s, 3H), 1.28–1.23 (m, 3H). ^{13}C NMR (126 MHz, DMSO-d_6) δ 165.91, 142.06, 141.63, 140.46, 140.00, 139.04, 138.13, 136.86, 132.32, 131.07, 130.30, 129.78 (d, J = 31.6 Hz), 129.31, 128.78, 127.36, 124.63 (d, J = 272.1 Hz), 124.26, 122.54, 120.77, 120.33, 119.60, 116.88, 115.05, 110.78, 65.95, 59.18, 21.43, 20.81.HRMS m/z (ESI) found 520.1946 (M + H)$^+$, $C_{28}H_{25}F_3N_5O_2^+$ calcd for 520.1955, retention time 3.59 min, 100% pure.

*5.1.14.1.14. 3-(3-(1-(2-(dimethylamino)-2-oxoethyl)-1H-pyrazol-4-yl)-1H-indazol-6-yl)-4-methyl-N-(3-(trifluoromethyl)phenyl)benzamide (**11n**).* White solid, Yield: 50%. ^{1}H NMR (400 MHz, DMSO-d_6) δ 13.06 (s, 1H), 10.52 (s, 1H), 8.34 (s, 1H), 8.25 (s, 1H), 8.08 (d, J = 8.3 Hz, 2H), 8.05 (s, 1H), 7.99 (s, 1H), 7.95 (d, J = 8.2 Hz, 1H), 7.60 (t, J = 8.0 Hz, 1H), 7.53 (m, 2H), 7.45 (d, J = 7.8 Hz, 1H), 7.22 (d, J = 8.4 Hz, 1H), 5.21 (s, 2H), 3.09 (s, 3H), 2.89 (s, 3H), 2.36 (s, 3H). ^{13}C NMR (126 MHz, DMSO-d_6) δ 167.07, 165.89, 142.04, 141.64, 140.47, 140.00, 139.06, 138.06, 136.99, 132.31, 131.08, 130.30, 129.78 (d, J = 31.5 Hz), 129.73, 129.29, 127.39, 124.63 (d, J = 272.2 Hz), 124.26,122.60, 120.69, 120.33, 119.60, 116.89, 115.48, 110.83, 53.34, 36.45, 35.72, 20.81. HRMS m/z (ESI) found 547.2076 (M + H)$^+$, $C_{29}H_{26}F_3N_6O_2^+$ calcd for 547.2064, retention time 3.58 min, >99% pure.

*5.1.14.1.15. 4-Methyl-3-(3-(1-(2-morpholinoethyl)-1H-pyrazol-4-yl)-1H-indazol-6-yl)-N-(3-(trifluoromethyl)phenyl)benzamide (**11o**).* Brown oil, Yield: 50%. ^{1}H NMR (400 MHz, Methanol-d_4) δ 8.33 (s,

1H), 8.19 (s, 1H), 8.11 (s, 1H), 8.04 (d, $J = 9.5$ Hz, 1H), 7.96 (d, $J = 8.6$ Hz, 1H), 7.93–7.88 (m, 2H), 7.54 (d, $J = 7.8$ Hz, 1H), 7.50 (s, 1H), 7.47 (d, $J = 7.1$ Hz, 1H), 7.42 (d, $J = 7.6$ Hz, 1H), 7.22 (d, $J = 8.4$ Hz, 1H), 4.40 (t, $J = 6.8$ Hz, 2H), 3.69 (t, $J = 4.5$ Hz, 4H), 2.89 (t, $J = 6.5$ Hz, 2H), 2.54 (t, $J = 4.5$ Hz, 4H), 2.36 (d, $J = 2.3$ Hz, 3H). HRMS *m/z* (ESI) found 575.2383 $(M + H)^+$, $C_{31}H_{30}F_3N_6O_2^+$ calcd for 575.2377, retention time 3.27 min, >99% pure.

*5.1.14.1.16. 4-Methyl-3-(3-(1-(tetrahydrofuran-3-yl)-1H-pyrazol-4-yl)-1H-indazol-6-yl)-N-(3-(trifluoromethyl)phenyl)benzamide (**11p**).* ^{1}H NMR (400 MHz, Methanol-d_4) δ 8.33 (s, 1H), 8.19 (s, 1H), 8.14 (s, 1H), 8.07 (d, $J = 8.3$ Hz, 1H), 7.96 (d, $J = 8.6$ Hz, 1H), 7.94–7.90 (m, 2H), 7.55 (t, $J = 8.1$ Hz, 1H), 7.52 (s, 1H), 7.50 (d, $J = 8.1$ Hz, 1H), 7.44 (d, $J = 7.8$ Hz, 1H), 7.25 (d, $J = 8.3$ Hz, 1H), 5.18 (dq, $J = 8.0$, 3.8 Hz, 1H), 4.21 (q, $J = 7.7$ Hz, 1H), 4.18–4.09 (m, 2H), 3.98 (td, $J = 8.4$, 5.6 Hz, 1H), 2.64–2.52 (m, 1H), 2.49–2.40 (m, 1H), 2.39 (s, 3H). ^{13}C NMR (126 MHz, DMSO-d_6) δ 165.91, 142.06, 141.65, 140.47, 139.98, 139.07, 138.12, 136.88, 132.33, 131.05, 130.27, 129.80 (d, $J = 31.5$ Hz), 129.32, 128.49, 127.36, 124.63 (d, $J = 272.4$ Hz), 124.25, 122.55, 120.74, 120.31 (d, $J = 4.3$ Hz), 119.62, 116.90 (q, $J = 3.9$ Hz), 115.17, 110.81, 66.68, 58.25, 53.62, 20.79.HRMS *m/z* (ESI) found 532,1951 $(M + H)^+$, $C_{29}H25F_3N_5O_2^+$ calcd for 532.1955, retention time 3.62 min, >99% pure.

*5.1.14.1.17. 4-Methyl-3-(3-(1-(tetrahydro-2H-pyran-2-yl)-1H-pyrazol-4-yl)-1H-indazol-6-yl)-N-(3-(trifluoromethyl)phenyl)benzamide (**11q**).* Pale yellow solid, Yield: 60%. ^{1}H NMR (400 MHz, Methanol-d_4) δ 8.36 (s, 1H), 8.20 (s, 1H), 8.14 (d, $J = 0.7$ Hz, 1H), 8.09 (dd, $J = 8.4$, 0.8 Hz, 1H), 7.96 (d, $J = 8.3$ Hz, 1H), 7.94–7.91 (m, 2H), 7.56 (t, $J = 8.0$ Hz, 1H), 7.53–7.47 (m, 2H), 7.44 (d, $J = 9.3$ Hz, 1H), 7.26 (dd, $J = 8.4$, 1.4 Hz, 1H), 4.65–4.47 (m, 1H), 4.22–4.03 (m, 2H), 3.64 (td, $J = 11.7$, 2.5 Hz, 2H), 2.40 (s, 3H), 2.28–2.07 (m, 4H). ^{13}C NMR (126 MHz, DMSO-d_6) δ 165.42, 141.59, 141.15, 139.98, 139.51, 138.57, 137.64, 136.20, 131.83, 130.58, 129.81, 129.30 (d, $J = 31.4$ Hz), 128.83, 126.88, 125.57, 124.15 (d, $J = 272.5$ Hz), 123.78, 122.02, 120.44, 119.85, 119.12, 116.42, 114.70, 110.26, 65.99, 57.40, 32.94, 26.82, 20.32.HRMS *m/z* (ESI) found 546.2125 $(M + H)^+$, $C_{30}H_{27}F_3N_5O_2^+$ calcd for 546.2111, retention time 3.85 min, >99% pure.

*5.1.14.1.18. 4-Methyl-3-(3-(1-(1-methylpiperidin-4-yl)-1H-pyrazol-4-yl)-1H-indazol-6-yl)-N-(3-(trifluoromethyl)phenyl)benzamide (**11r**).* Grey solid, Yield: 57%. ^{1}H NMR (400 MHz, Methanol-d4) δ 8.38 (s, 1H), 8.21 (d, $J = 1.9$ Hz, 1H), 8.16 (s, 1H), 8.08 (d, $J = 8.4$ Hz, 1H), 7.98–7.93 (m, 1H), 7.93–7.89 (m, 2H), 7.56 (d, $J = 8.0$ Hz, 1H), 7.54–7.51 (m, 1H), 7.48 (d, $J = 8.2$ Hz, 1H), 7.43 (d, $J = 7.7$ Hz, 1H), 7.24 (dd, $J = 8.3$, 1.4 Hz, 1H), 4.66 (m, 1H), 3.27–3.18 (m, 2H), 2.91 (s, 3H), 2.45 (m, 4H), 2.37 (s, 3H),1.28–1.36 (m, 2H). ^{13}C NMR (126 MHz, DMSO-d_6) δ 165.42, 141.60, 141.14, 139.98, 139.51, 138.55, 137.68, 136.13, 131.83, 130.58, 129.81, 129.30 (d, $J = 31.5$ Hz), 128.82, 126.87, 125.64, 124.15 (d, $J = 272.3$ Hz), 123.77,122.01, 120.45, 119.86, 119.12, 116.38, 114.59, 110.25, 54.16, 45.68, 31.95, 26.82, 20.32.LRMS *m/z*: 559.4 ([M+H] $^+$). HRMS *m/z* (ESI) found 559.2433$(M + H)^+$, $C_{31}H_{30}F_3N_6O^+$ calcd for 559.2428, retention time 3.25 min, 100% pure.

*5.1.14.1.19. 4-Methyl-N-(3-((4-methylpiperazin-1-yl)methyl)-5-(trifluoromethyl)phenyl)-3-(4,4,5,5-tetramethyl-1,3,2-dioxaborolan-2-yl)benzamide(**28**).* To a resealable vial was added AcOK (188 mg, 1.91 mmol), **25k** (300 mg, 0.638 mmol), Bis(pinacolato)diboron (243 mg, 0.957 mmol). The vial was sealed and evacuated and purged with Ar for 5min before addition of $PdCl_2$(dppf)-CH_2Cl_2 Adduct (26 mg, 0.032 mmol), dissolved in DMSO (20 mL) was then added to this solution before the vial was heated to 80 °C for 5 h. The reaction mixture was diluted with ethyl acetate and washed with a saturated aqueous sodium bicarbonate solution and saline. The organic layer thus obtained was dried over anhydrous sodium sulfate, filtered, and concentrated under reduced pressure. The resulting mixture was concentrated to give the crude product, which was purified by silica gel column chromatography (eluting with 0–20% MeOH in DCM) to provide **28**. Brown Oil, Yield: 78%.^{1}H NMR (400 MHz, Methanol-d4) δ 8.32 (s, 1H), 8.07 (s, 1H), 7.97 (s, 1H), 7.91 (d, $J = 8.1$ Hz, 2H), 7.44 (s, 1H), 7.35 (d, $J = 8.1$ Hz, 1H), 3.66 (s, 2H), 2.70 (brs, 8H), 2.61 (s, 3H), 2.44 (s, 3H), 1.40 (s, 12H). LRMS *m/z*: 559.4 ([M+H] $^+$).

*5.1.14.1.20. 3-(3-(1-cyclopropyl-1H-pyrazol-4-yl)-1H-indazol-6-yl)-4-methyl-N-(3-((4-methylpiperazin-1-yl)methyl)-5-(trifluoromethyl)phenyl)benzamide (**12**).* To a resealable vial was added **28** (427 mg, 0. 825 mmol), K_2CO_3 (228 mg, 1.65 mmol) and **27k** (250 mg, 0.825 mmol). The vial was sealed and evacuated and purged with Ar for 5 min before addition of $PdCl_2$(dppf)-CH_2Cl_2 adduct (35 mg, 0.041 mmol), dissolved in 1,4-dioxane/water (10 mL, 4:1, v/v) was then added to this solution before the vial was heated to 80 °C overnight. The reaction was cooled to room temperature, which was then brought to basic using aqueous sodium bicarbonate solution and extracted with ethyl acetate. The resulting mixture was concentrated to give the crude product, which was purified by silica gel column chromatography. The crude residue was purified via by silica gel column chromatography (eluting with 0–10% MeOH in DCM) to afford the product as white solid (267 mg, 53%). LC–MS *m/z* (ESI) found 614.11$(M + H)^+$; ^{1}H NMR (400 MHz, Methanol-d4) δ 8.31 (s, 1H), 8.08 (dd, $J = 4.8$, 0.8 Hz, 2H), 8.06–8.04 (m, 1H), 8.02 (d, $J = 1.7$ Hz, 1H), 7.92 (d, $J = 7.3$ Hz, 2H), 7.51 (d, $J = 1.2$ Hz, 1H), 7.51–7.47 (m, 1H), 7.44 (s, 1H), 7.23 (dd, $J = 8.4$, 1.4 Hz, 1H), 3.78 (tt, $J = 7.3$, 3.8 Hz, 1H), 3.68 (s, 2H), 3.02 (s, 4H), 2.67 (s, 7H), 2.38 (s, 3H), 1.25–1.19 (m, 2H), 1.16–1.11 (m, 2H). ^{13}C NMR (126 MHz, Methanol-*d*4) δ 168.69, 143.69, 142.93, 141.59, 141.40, 141.09, 140.94, 139.39, 138.35, 133.33, 132.27 (d, $J = 32.2$ Hz), 131.84, 130.17, 129.38, 127.81, 125.81, 125.52 (d, $J = 271.7$ Hz), 123.97, 122.17, 121.57, 120.81, 117.61, 116.33, 111.56, 62.41, 55.27, 51.92, 44.47, 33.79, 20.80, 7.07. HRMS *m/z* (ESI) found 614.2865 $(M + H)^+$, $C_{34}H_{35}F_3N_7O^+$ calcd for 614.285; retention time 3.01min, 100% pure.

5.2. ELISA kinase assay

The effects of indicated compound on the activities of various tyrosine kinases were determined using enzyme-linked immunosorbent assays (ELISAs) with purified recombinant proteins. Briefly, 20 μg/mL poly (Glu, Tyr) $_{4:1}$ (Sigma, St Louis, MO, USA) was pre-coated in 96-well plates as a substrate. A 50-μL aliquot of 10 μM ATP solution diluted in kinase reaction buffer (50 mM HEPES [pH 7.4], 50 mM $MgCl_2$, 0.5 mM $MnCl_2$, 0.2 mM Na_3VO_4, and 1 mM DTT) was added to each well; 1 μL of indicated compound diluted in 1% DMSO (v/v) (Sigma, St Louis, MO, USA) were then added to each reaction well. DMSO (1%, v/v) was used as the negative control. The kinase reaction was initiated by the addition of purified tyrosine kinase proteins diluted in 49 μL of kinase reaction buffer. After incubation for 60 min at 37 °C, the plate was washed three times with phosphate-buffered saline (PBS) containing 0.1% Tween 20 (T-PBS). Anti-phosphotyrosine (PY99) antibody (100 μL; 1:500, diluted in 5 mg/mL BSA T-PBS) was then added. After a 30-min incubation at 37 °C, the plate was washed three times, and 100 μL horseradish peroxidase-conjugated goat anti-mouse IgG (1:1000, diluted in 5 mg/mL BSA T-PBS) was added. The plate was then incubated at 37 °C for 30 min and washed 3 times. A 100-μL aliquot of a solution containing 0.03% H_2O_2 and 2 mg/mL *o*-phenylenediamine in 0.1 M citrate buffer (pH 5.5) was added. The reaction was terminated by the addition of 50 μL of 2 M H_2SO_4 as the color changed, and the plate was analyzed using a multi-well spectrophotometer (SpectraMAX190, from Molecular Devices, Palo Alto, CA, USA) at 490 nm. The inhibition rate (%) was calculated using the following equation: [1-(A490/A490 $_{control}$)] × 100%. The IC_{50} values were calculated from the inhibition curves in two separate experiments.

5.3. Molecular modeling

The 3D structure of DDR2 kinase domain (aa. 557–851) were built by the online homology modeling server (www. swissmodel.expasy.org), with the crystal structure of DDR1 (PDB ID: 4CKR) as the template. All the default parameters implemented in the server were adopted, and the statistics of final 3D model structure indicated the model structure is suitable for further docking study. Then, the DDR2 model structure and FGFR1 crystal structure (PDB ID: 4V04) were processed with protein preparation module in Schrödinger software package, and ATP binding site were selected for making the grid file with Glide module. Then the ligands were prepared to add the partial charge, minimize to obtain the low-energy conformation. Finally, ligands were docked into the grid files with default parameters at standard precision mode, and the predicted binding modes were depicted with Pymol software.

5.4. Cell culture

Human lung cancer cell lines NCI-H1581, NCI-H12286, human acute myelogenous leukemia cell lines KG-1, human gastric cancer cell lines SNU-16 and human bladder cancer cell lines NCI-H716 were purchased from American Type Culture Collection (ATCC, Manassas, VA, USA). Human bladder cancer cell lines UMUC14 was purchased from European Collection of Cell Cultures (ECACC). All the cell lines were routinely maintained in media according to the suppliers' recommendations. All cell lines were authenticated via short tandem repeats analysis by Genesky Biopharma Technology (last tested in 2016).

5.5. Western blot analysis

SNU-16 and NCI-H2286 cells were treated with the indicated dose of compounds for 2 h at 37 °C and then lysed in 1 × SDS sample buffer. The cell lysates were subsequently resolved by 10% SDS-PAGE and transferred to nitrocellulose membranes. The membranes were probed with the appropriate primary antibodies [phospho-FGFR, FGFR2, phosphor–DDR2, DDR2, phosphor-ERK, ERK, phosphor-Akt, Akt, GAPDH (all from Cell Signaling Technology, Beverly, MA, USA)] and then with horseradish peroxidase-conjugated anti-rabbit or anti-mouse IgG. The immune reactive proteins were detected using an enhanced chemilluminescense detection reagent (Thermo Fisher Scientific, Rockford, IL, USA).

5.6. Cell proliferation assays

Cells were seeded in 96-well plates at a low density in growth media. The next day, appropriate controls or designated concentrations of compounds were added to each well, and the cells were incubated for 72 h. Finally, cell proliferation was determined using a sulforhodamine B assay, a thiazolyl blue tetrazolium bromide assay or a cell counting kit (CCK-8) assay. IC_{50} values were calculated by concentration-response curve fitting using a SoftMax pro-based four-parameter method.

5.7. In vivo antitumor activity assay

Female nude mice (4–6 weeks old) were housed and maintained under specific pathogen-free conditions. Animal procedures were performed according to institutional ethical guidelines of animal care. The tumor cells at a density of 5×10^6 in 200 μL were injected subcutaneously (s.c.) into the right flank of nude mice and then allowed to grow to 700–800 mm^3, which was defined as a well-developed tumor. Subsequently, the well-developed tumors were cut into 1-mm^3 fragments and transplanted s.c. into the right flank of nude mice using a trocar. When the tumor volume reached 100–150 mm^3, the mice were randomly assigned into a vehicle control group (n = 12 or 10) and treatment groups (n = 6 or 5 per group). The control group was given only vehicle, and the treatment groups received compounds at the indicated doses via oral injection once daily for 7 or 10 days. The sizes of the tumors were measured twice per week using a microcaliper. Tumor volume (TV) = (length × $width^2$)/2, and the tumor volume was shown on indicated days as the Mean ± SE indicated for groups of mice. Percent (%) inhibition(TGI)values were measured on the final day of study for the drug-treated mice compared with vehicle-treated mice and were calculated as $100 \times \{1 - [(TV_{Treated\ Final\ day} - TV_{Treated\ Day\ 0})/(TV_{Control\ Final\ day} - TV_{Control\ Day\ 0})]$.Significant differences between the treated versus the control groups ($P \leq 0.05$) were determined using Student's *t*-test.

5.8. In vitro analysis of Caco-2 permeability

Assays to monitor uptake and efflux of compounds by polarized epithelial cells were conducted by Absorption Systems Inc. In brief, Caco-2 cells (Clone C2BBel from ATCC) were grown to confluence on collagen-coated polycarbonate membranes on transwell plates. Permeability assays were conducted in Hank's balanced salt solution, containing 10 mM HEPES, 10 mM HBSS, pH 7.4 and PH 6.8. Compounds were added at 5 μM to the apical (A) vs basolateral (B) side, and duplicate samples were taken at 120 min. Samples were analyzed by LC-MS/MS and expressed as apparent permeability (Papp) for uptake (A to B) vs efflux (B to A) and efflux ratio (Papp(B to A)/Papp(A to B)).

5.9. In vitro liver microsome assay and P450 enzymatic inhibition assay

Microsomes (0.5 mg/mL) were preincubated with 1 mM test compound for 5 min at 37 °C in 0.1 M phosphate buffer (pH 7.4) with 1 mM of EDTA and 5 mM of $MgCl_2$. The reactions were started by adding cofactors (1 mM of NADPH). After 0, 5, 10, and 30 min incubations at 37 °C, the reactions were stopped by adding an equal volume of cold acetonitrile. The samples were vortexed for 10 min and then centrifuged at 15,000 rmp for 10 min. Supernatants were analyzed by LC/MS/MS for the amount of parent compound remaining, and the corresponding loss of parent compound was also determined by LC/MS/MS.

The CYP enzymatic activities were characterized based on their probe reactions: CYP3A4 (midazolam or testosterone), CYP2D6 (dextromethorphan), CYP2C9 (Diclofenac), CYP1A2 (phenacetin), and CYP2C19 (Mephenytoin). Incubation mixtures were prepared in a total volume of 100 mL as follows: 0.2 mg/mL microsome, 1 mmol of NADPH, 100 mmol of pH7.4 phosphate buffer, probe substrates cocktail (10 μM midazolam, 100 μM testosterone, 10 μM dextromethophan, 20 μM diclofenac, 100 μM phenacetin, and 100 μM Mephenytoin) and 10 mM tested compound or positive control cocktail (10 μM ketoconazole, 10 μM quinidine, 100 μM sulfaphenazole, 10 μM naphthoflavone, and 1000 μM Mtranylcypromine) or negative control (PBS). The final concentration of organic reagent in incubation mixtures was less than 1% v/v. There was a 5 min preincubation period at 37 °C before the reaction was initiated by adding a NADPH generating system. Reactions were conducted for 20 min for CYPs. For each probe drug, the percentage of metabolite conversion was less than 20% of substrate added. The inhibition rate was calculated as (the formation of the metabolite of probe substrates with 10 μM tested compound)/(the formation of the metabolite of probe substrates with PBS) × 100%.

The CYP enzymatic activities were characterized based on their probe reactions: CYP3A4 (midazolam or testosterone), CYP2D6

(dextromethorphan), CYP2C9 (Diclofenac), CYP1A2 (phenacetin), and CYP2C19 (S-(+)-mephenytoin). Incubation mixtures were prepared in a total volume of 200 μl as follows: 0.2 mg/mLmicrosome, 1 mM of NADPH, 100 mM of pH7.4 phosphate buffer, 10 μM tested compound, positive control cocktail (10 mM troleandomycin, 10 μM paroxetine, 10 μM tienilic Acid, 10 μM furafylline) or negative control (PRO). The final concentration of organic reagent in incubation mixtures was less than 1% v/v. There was a 0min, 5min,10min and 30min preincubation period at 37 °C before the reaction was initiated by adding a NADPH and probe substrates cocktail (5 μM midazolam, 50 μM testosterone, 5 μM dextromethophan, 10 μM diclofenac, 50 μM phenacetin, and 50 μM S-(+)-mephenytoin) generating system. Reactions were conducted for 10 min for CYPs. The CYP2C19 enzyme was made alone, and the concentration of positive control cocktail S-(+)-fluoxetine was 100 μM. For each probe drug, the percentage of metabolite conversion was less than 20% of substrate added. The inhibition rate was calculated as (the formation of the metabolite of probe substrates with 10 μM tested compound)/(the formation of the metabolite of probe substrates with PRO) × 100%.

5.10. Mouse pharmacokinetics study

Compounds dissolved in 1% Tween80/water to a concentration of 1 mg/mL, and was given to ICR mice (Male, 18–22 g, n = 3) by gavage administration. Animal procedures were performed according to institutional ethical guidelines of animal care. Blood samples were collected at 0.25, 0.5, 1, 2, 4, 8, and 24 h after administration.100 mL of solvent of methanol: acetonitrile (1:1, v/v) with internal standard was added to 10 mL of plasma and vortexed thoroughly. It was centrifuged for 5 min, then 20 mL of the supernatant was mixed with 20 mL of water for analysis. Samples were analyzed by Xevo TQ-S triple quadrupole mass spectrometer. The ACQUITY UPLC BEH C18 (1.7 μm, 2.0 mm_ 50 mm, Waters, USA) was used for the analysis. Gradient elution was applied consisting of 5 mM ammonium acetate aqueous solution containing 0.1% formic acid and acetonitrile containing 0.1% formic acid. After analyzing the concentrations of these compounds, the value of AUClast, AUCINF_obs and MRTINF_obs was calculated from time-concentration curves in each animal using Phoenix WinNonlin (CERTARA, USA). C_{max} was determined as the maximum plasma concentration, and Tmax was the time to reach the maximum concentration.

Acknowledgement

We are grateful for financial support from the National Natural Science Foundation of China (Grant No. 81330076, 81773762) and the “Personalized Medicines—Molecular Signature-based Drug Discovery and Development”, Strategic Priority Research Program of the Chinese Academy of Sciences (Grant No. XDA12020323) and the National Science & Technology Major Project “Key New Drug Creation and Manufacturing Program” of China (Grant No. 2018ZX09711002-004).

Appendix A. Supplementary data

Supplementary data to this article can be found online at https://doi.org/10.1016/j.ejmech.2018.12.015.

References

[1] R.L. Siegel, K.D. Miller, A. Jemal, Cancer statistics, CA A Cancer J. Clin. 68 (2018) 7–30, 2018.
[2] W.D. Travis, E. Brambilla, A.P. Burke, A. Marx, A.G. Nicholson, Introduction to the 2015 world health organization classification of tumors of the lung, pleura, thymus, and heart, J. Thorac. Oncol. 10 (2015) 1240–1242.
[3] W.D. Travis, E. Brambilla, A.G. Nicholson, Y. Yatabe, J.H.M. Austin, M.B. Beasley, L.R. Chirieac, S. Dacic, E. Duhig, D.B. Flieder, K. Geisinger, F.R. Hirsch, Y. Ishikawa, K.M. Kerr, M. Noguchi, G. Pelosi, C.A. Powell, M.S. Tsao, I. Wistuba, W.H.O. Panel, The 2015 world health organization classification of lung tumors: impact of genetic, clinical and radiologic advances since the 2004 classification, J. Thorac. Oncol. 10 (2015) 1243–1260.
[4] B.A. Chan, B.G. Hughes, Targeted therapy for non-small cell lung cancer: current standards and the promise of the future, Transl. Lung Cancer Res. 4 (2015) 36–54.
[5] C. Lazzari, N. Karachaliou, V. Gregorc, A. Bulotta, M. Gonzalez-Cao, A. Verlicchi, G. Altavilla, R. Rosell, M. Santarpia, Second-line therapy of squamous non-small cell lung cancer: an evolving landscape, Expert Rev. Respir. Med. 11 (2017) 469–479.
[6] K. Koutsoukos, G. Mountzios, Novel therapies for advanced squamous cell carcinoma of the lung, Future Oncol. 12 (2016) 659–667.
[7] P. Savas, B. Hughes, B. Solomon, Targeted therapy in lung cancer: IPASS and beyond, keeping abreast of the explosion of targeted therapies for lung cancer, J. Thorac. Dis. 5 (Suppl 5) (2013) S579–S592.
[8] H.S. Kim, T. Mitsudomi, R.A. Soo, B.C. Cho, Personalized therapy on the horizon for squamous cell carcinoma of the lung, Lung Canc. 80 (2013) 249–255.
[9] Therapeutic options in advanced squamous cell lung carcinoma.
[10] Y. Bai, J.Y. Kim, J.M. Watters, B. Fang, F. Kinose, L. Song, J.M. Koomen, J.K. Teer, K. Fisher, Y.A. Chen, U. Rix, E.B. Haura, Adaptive responses to dasatinib-treated lung squamous cell cancer cells harboring DDR2 mutations, Cancer Res. 74 (2014) 7217–7228.
[11] J.D. Campbell, A. Alexandrov, J. Kim, J. Wala, A.H. Berger, C.S. Pedamallu, S.A. Shukla, G. Guo, A.N. Brooks, B.A. Murray, M. Imielinski, X. Hu, S. Ling, R. Akbani, M. Rosenberg, C. Cibulskis, A. Ramachandran, E.A. Collisson, D.J. Kwiatkowski, M.S. Lawrence, J.N. Weinstein, R.G. Verhaak, C.J. Wu, P.S. Hammerman, A.D. Cherniack, G. Getz, N. Cancer Genome Atlas Research, M.N. Artyomov, R. Schreiber, R. Govindan, M. Meyerson, Distinct patterns of somatic genome alterations in lung adenocarcinomas and squamous cell carcinomas, Nat. Genet. 48 (2016) 607–616.
[12] S.J. An, Z.H. Chen, J. Su, X.C. Zhang, W.Z. Zhong, J.J. Yang, Q. Zhou, X.N. Yang, L. Huang, J.L. Guan, Q. Nie, H.H. Yan, T.S. Mok, Y.L. Wu, Identification of enriched driver gene alterations in subgroups of non-small cell lung cancer patients based on histology and smoking status, PLoS One 7 (2012), e40109.
[13] N. Turner, R. Grose, Fibroblast growth factor signalling: from development to cancer, Nat. Rev. Canc. 10 (2010) 116–129.
[14] N. Cihoric, S. Savic, S. Schneider, I. Ackermann, M. Bichsel-Naef, R.A. Schmid, D. Lardinois, M. Gugger, L. Bubendorf, I. Zlobec, C. Tapia, Prognostic role of FGFR1 amplification in early-stage non-small cell lung cancer, Br. J. Canc. 110 (2014) 2914–2922.
[15] H.L. Fu, R.R. Valiathan, R. Arkwright, A. Sohail, C. Mihai, M. Kumarasiri, K.V. Mahasenan, S. Mobashery, P. Huang, G. Agarwal, R. Fridman, Discoidin domain receptors: unique receptor tyrosine kinases in collagen-mediated signaling, J. Biol. Chem. 288 (2013) 7430–7437.
[16] L.A. Walsh, A. Nawshad, D. Medici, Discoidin domain receptor 2 is a critical regulator of epithelial-mesenchymal transition, Matrix Biol. 30 (2011) 243–247.
[17] L.S. Payne, P.H. Huang, Discoidin domain receptor 2 signaling networks and therapy in lung cancer, J. Thorac. Oncol. 9 (2014) 900–904.
[18] E. Bonastre, E. Brambilla, M. Sanchez-Cespedes, Cell adhesion and polarity in squamous cell carcinoma of the lung, J. Pathol. 238 (2016) 606–616.
[19] A.F. Gazdar, F.R. Hirsch, J.D. Minna, From mice to men and back: an assessment of preclinical model Systems for the study of lung cancers, J. Thorac. Oncol. 11 (2016) 287–299.
[20] A.P. Singh, D. Adrianzen Herrera, Y. Zhang, R. Perez-Soler, H. Cheng, Mouse models in squamous cell lung cancer: impact for drug discovery, Expert Opin. Drug Discov. 13 (4) (2018) 347–358.
[21] H.Y.T. Shimada, M. Mimura, Y. Inui, F.P. Guengerich, Interindividual variations in human liver cytochrome P-450 enzymes involved in the oxidation of drugs, carcinogens and toxic chemicals: studies with liver microsomes of 30 Japanese and 30 Caucasians, J. Pharmacol. Exp. Therapeut. 270 (1994) 414–423.